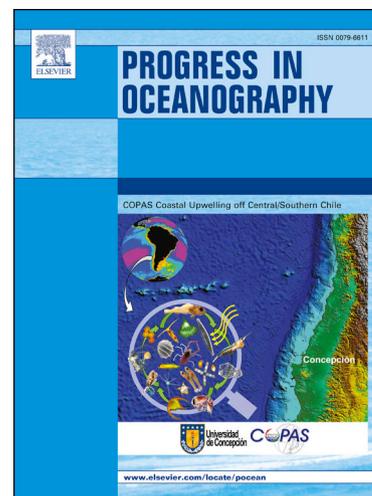# Accepted Manuscript

High-resolution net and gross biological production during a Celtic Sea spring bloom

Isabel Seguro, Alina D. Marca, Suzanne J. Painting, Jamie D. Shutler, David J. Suggett, Jan Kaiser

Please cite this article as: Seguro, I., Marca, A.D., Painting, S.J., Shutler, J.D., Suggett, D.J., Kaiser, J., High-resolution net and gross biological production during a Celtic Sea spring bloom, *Progress in Oceanography* (2017), doi: https://doi.org/10.1016/j.pocean.2017.12.003

This is a PDF file of an unedited manuscript that has been accepted for publication. As a service to our customers we are providing this early version of the manuscript. The manuscript will undergo copyediting, typesetting, and review of the resulting proof before it is published in its final form. Please note that during the production process errors may be discovered which could affect the content, and all legal disclaimers that apply to the journal pertain.

High-resolution net and gross biological production during a Celtic Sea spring bloom

Isabel Seguro (1), Alina D. Marca (1), Suzanne J. Painting (2), Jamie D. Shutler (3), David J. Suggett (4), Jan Kaiser (1)

[1] Centre for Ocean and Atmospheric Science, School of Environmental Sciences, University of East Anglia, UK. E-mail: i.seguro-requejo@uea.ac.uk

[2] Centre for Environment, Fisheries and Aquaculture Science, Lowestoft, UK

[3] Centre for Geography, Environment and Society, College of Life and Environmental Sciences, University of Exeter, Penryn Campus, UK

[4] Climate Change Cluster, University of Technology Sydney, NSW, Australia

Abstract

Shelf seas represent only 10 % of the ocean area, but support up to 30 % of all oceanic primary production. There are few measurements of shelf-sea biological production at high spatial and temporal resolution in such heterogeneous and physically dynamic systems. Here, we use dissolved oxygen-to-argon (O_2/Ar) ratios and oxygen triple isotopes (^{16}O, ^{17}O, ^{18}O) to estimate net and gross biological production in the Celtic Sea during spring 2015. O_2/Ar ratios were measured continuously using a shipboard membrane inlet mass spectrometer (MIMS). Additional discrete water samples from CTD hydrocasts were used to measure O_2/Ar depth profiles and the $\delta(^{17}O)$ and $\delta(^{18}O)$ values of dissolved O_2. These high-resolution data were combined with wind-speed based gas exchange parameterisations to calculate biologically driven air-sea oxygen fluxes. After correction for disequilibrium terms and diapycnal diffusion, these fluxes yielded estimates of net community ($N(O_2/Ar)$) and gross O_2 production ($G(^{17}O)$). $N(O_2/Ar)$ was spatially heterogeneous and showed predominantly autotrophic conditions, with an average of (33 ± 41) mmol m^{-2} d^{-1}. $G(^{17}O)$ showed high variability between 0 and 424 mmol m^{-2} d^{-1}. The ratio of $N(O_2/Ar)$ to $G(^{17}O)$, $f(O_2)$, was (0.18 ± 0.03) corresponding to 0.34 ± 0.06 in carbon equivalents. We also observed rapid temporal changes in $N(O_2/Ar)$, e.g. an increase of 80 mmol m^{-2} d^{-1} in less than 6 hours during the spring bloom, highlighting the importance of high-resolution biological production measurements. Such measurements will help reconcile the differ-

ences between satellite and in situ productivity observations, and improve our understanding of the biological carbon pump.

1. Introduction

Phytoplankton primary production is the main mechanism of oceanic carbon fixation. Although shelf seas comprise only 10 % of the world's oceans by area, they contribute 15 to 30 % of ocean primary production (Hickman et al., 2012). This disproportionately high productivity yields 90 % of the global fish catch (Pauly et al., 2002). Fish catch models greatly rely on net primary production estimates. Providing these models with inaccurate data or an incomplete understanding of the food web (e.g. the efficiency of trophic transfer) would hinder the ability of these models to project variability in primary production under future climate change (Stock et al., 2017) or due to changes in other anthropogenic and natural factors (CO_2 emissions, sewage, maritime transit, industrial waste, continental runoff, river discharge). Quantifying primary production is also of central importance to understanding the shelf sea carbon pump, and its role in the uptake of anthropogenic CO_2 emissions from the atmosphere (Thomas et al., 2005). The discussion on how our seas will react to anthropogenic forcing and climate change would therefore benefit from high-resolution primary production measurements adapted to the complex dynamics of shelf seas.

Temperate shelf seas are relatively well sampled and studied (see also other papers in this special issue). The highest primary productivity in temperate shelf seas typically occurs in spring (e.g. Barnes et. al. 2015). However, quantitative estimates of primary production are often highly divergent (Holligan et al., 1984; Joint & Pomroy, 1983; Joint, 1986; Rees et al., 1999; Robinson et al., 2009), confounding efforts to better understand inherent patterns and drivers of spatial and temporal variability. In part, this gap in knowledge reflects that different methods are often difficult to reconcile given that they quantify different quantities related to photosynthesis (Reuer et al., 2007; Robinson et al., 2009; Suggett et al., 2009). Also, most methods used, notably ^{14}C, ^{18}O and ^{15}N assimilation methods, light-dark bottle method using O_2 concentrations or closed-chamber CO_2 fluxes, are snap shots at the time and place sampled and require discrete incubations that are unlikely to represent the natural conditions in the inherently highly dynamic context of shelf seas (Quay et al., 2012; Sharples et al., 2006).

Novel approaches of continuous in situ measurements can resolve temporal and spatial variability over large areas, e.g. fast repetition rate fluorometry (FRRF). This technique has been adopted to better evaluate how productivity changes over space and time (Moore et al., 2006), but suffers from fundamental challenges in reconciling

its results with actual O_2 evolution or carbon uptake where environmental conditions are highly changeable. Satellite ocean colour remote sensing can provide synoptic scale observations of production at or near the surface of the water, but most current satellite sensors only provide these observations 1-2 times a day during cloud-free conditions. Also, recent studies show that chlorophyll *a* concentration mismatches with in situ measurements in shelf seas are in part due to errors in satellite estimates, which lead to bias in phytoplankton productivity (Stock et al., 2017). Therefore, satellite estimates require better validation against independent in situ observations (Campbell et al., 2002).

In the last 15 years, considerable efforts have been made in developing and improving techniques to measure marine biological productivity (Cassar et al., 2009; Juranek & Quay, 2013; Kaiser et al., 2005; Tortell, 2005). There are different terms and metrics in use to express marine biological productivity (or production), in particular gross and net primary production (GPP, NPP) and net community production (NCP), either expressed in terms of C or O_2 equivalents. GPP, here measured as $G(^{17}O)$, represents the total photosynthetic O_2 production by autotrophs. NCP, here measured as $N(O_2/Ar)$, is GPP minus community respiration by autotrophs and heterotrophs. NPP is GPP minus autotrophic respiration, an approximation of which is derived from 24 hour ^{14}C incubations, here designated $P(^{14}C; 24\ h)$.

Despite spatio-temporal limitations during a research cruise and inherent uncertainties to any productivity determination, the non-incubation methods based on dissolved oxygen-to-argon (O_2/Ar) ratios and triple oxygen isotopes (^{16}O, ^{17}O, ^{18}O) provide an improved way to derive estimates of net and gross biological production (Juranek & Quay, 2013; Quay et al., 2012). These two methods together can be used to estimate the efficiency of the carbon pump (Haskell et al., 2017; Palevsky et al., 2016), based on the ratio of $N(O_2/Ar)$ to $G(^{17}O)$, or $f(O_2)$.

Here, we use the biogeochemical O_2/Ar method to derive mixed layer net community production rates from continuous membrane inlet mass spectrometry (MIMS) measurements (Kaiser et al., 2005), which resolves variability at sub-km scale resolution. Using the measured O_2/Ar supersaturation and wind-speed based air-sea gas exchange parameterisations, we calculate biological O_2 air-sea fluxes (F_{bio}), correct them for diapycnal diffusion and disequilibrium terms to estimate mixed layer net community production rates. These measurements are combined with shore-based analyses of discrete samples for oxygen triple isotope ratios to derive gross O_2 production rates

4

(Luz et al., 1999). Our combined approach results in high-resolution in situ estimates of primary production during the spring bloom in the Celtic Sea. Such measurements can serve to validate satellite ocean colour productivity estimates, and feed models of the carbon pump to predict the impact of climate change. This will improve our understanding of primary production variability and potential impacts of human activities in the temperate shelf seas.

2. Material and Methods

2.1 Study area

The temperate Celtic Sea comprises an area of the North Atlantic Ocean and is part of the northwest European shelf. Throughout the Celtic Sea, the spring bloom typically initiates in April when the water column becomes stratified, and can last anywhere from weeks to two months (Rees et al., 1999; Sharples et al., 2006). The barotropic M_2 tide is responsible for the predominant currents in this region, which are considered weak and spatially variable compared with the adjacent areas of the European Shelf Sea (Holt et al., 2001). We sampled during the DY029 "spring cruise" in April 2015, as part of the NERC Shelf-Sea Biogeochemistry (SSB) programme. MIMS O_2/Ar data collection started in the English Channel and continued almost uninterrupted for 28 days in the Celtic Sea, focussing on repeat transects between Celtic Deep (station A) and Shelf Edge (stations CS2 and Fe). Discrete samples were taken from Niskin bottles attached to a CTD rosette water sampler at all stations (Fig. 1).
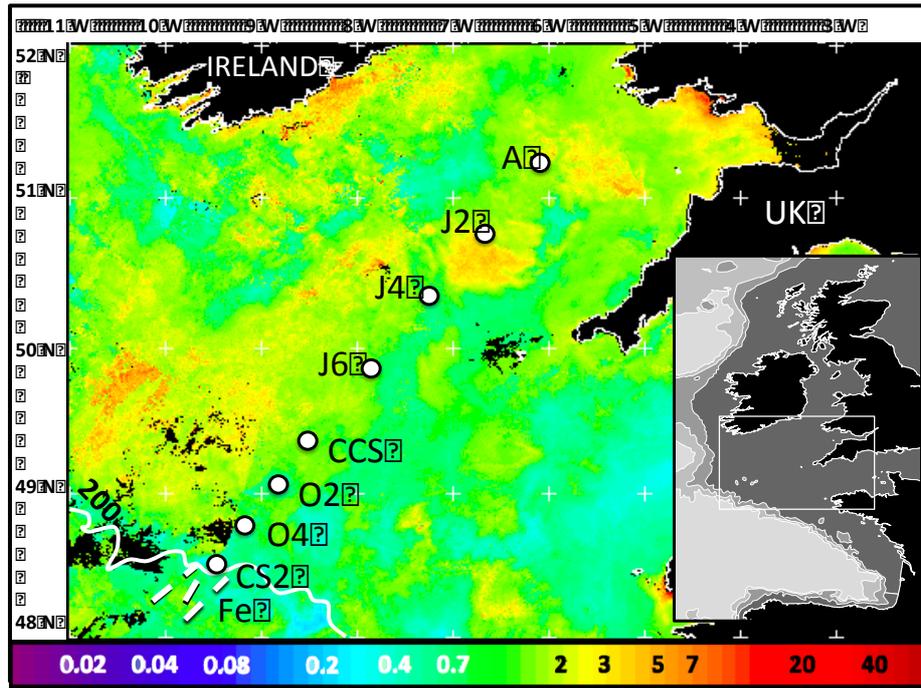
Fig. 1. Area of study in the Celtic Sea, with Ireland in the north and Great Britain in the east. White circles, superimposed on a chlorophyll *a* concentration (in mg m^{-3}) composite image from VIIRS Chlorophyll OC5 (11th to 19th of April; courtesy of NEODAAS), indicate the approximate station locations (A, J2, J4, J6, CCS, O2, O4, CS2). Straight white blocks represent multiple stations outside the shelf (Fe). The curved white line between CS2 and Fe indicates the shelf-edge, represented by the 200 metre isobath. The contextual wider area map (grey inset) was plotted using QGIS software.

2.2 Methods

Along-track O$_2$/Ar ratios were determined using a shipboard MIMS connected to the ship's non-toxic underway seawater (USW) intake. We also collected discrete samples for triple oxygen isotopes that were subsequently analysed with a dual-inlet isotope ratio mass spectrometer (IRMS Finnigan MAT 252) in the Stable Isotope Laboratory at the University of East Anglia.

Continuous sampling

The USW intake was located in the middle of the bow at a nominal depth of 6 m, and plumbed to the main laboratory. To avoid biofouling (Juranek et al., 2010), the USW pipes were treated with dilute bleach solution and flushed immediately prior to the

cruise and after two weeks at sea. Comparison between samples collected from near-surface Niskin bottles and USW samples, measured by IRMS, showed no consumption or production of oxygen in our ship's pipes.

The MIMS was set-up according to Kaiser et al. (2005), but with the vacuum on the inside of the membrane and modified flow (45 ml/min) and temperature control. Before entering the membrane inlet, a small open flask (500 ml) was used to smooth fluctuations in the pumped seawater delivery (1 L min^{-1}). The flow to the membrane inlet was delivered by a gear pump (*Micropump*) controlled by a frequency inverter (*Allen-Bradley*). The USW circuit in the lab and the membrane (Teflon AF membrane, Random Technologies) were maintained at 1 to 3 ºC below sea surface temperature, to avoid degassing. The temperature of the mass spectrometer flight tube was kept constant at 50 °C using an insulated box with an electric heater and fan inside. Standards of 0.2 μm-filtered seawater, aerated and stirred for 24 hours to reach air-saturation were used for daily calibration. Standard error in O_2/Ar of 0.09 %. O_2/Ar ion current ratios were measured with a quadrupole mass spectrometer QMS 200 M Prisma (*Pfeiffer Vacuum*) with Faraday cup and recorded every ten seconds. The analyser was at a constant pressure of 1.0×10^{-6} mbar.

The shipboard MIMS calibration was cross-checked against O_2/Ar ratios derived from discrete samples extracted and analysed as described in the next paragraph. Both calibrations gave identical results, with a mean difference of $\Delta(O_2/Ar)$ between discrete and continuous measurements of (0.0±0.6) % (1σ; $R^2 = 0.98$, $n = 142$).

Discrete sampling

We also took discrete samples from 33 CTD Niskin casts at six different depths (three in the surface mixed layer and three below) and measured their O_2/Ar ratio with the MIMS. During analysis of these samples, flow was alternated between continuous USW supply and discrete samples using a six-port valve (*Valco Cheminert*).

Further discrete samples from the same CTD casts as mentioned above were taken to measure oxygen triple isotopes and O_2/Ar ratios from three depths, (surface, near the bottom of the surface mixed layer, and below the surface mixed layer), using evacuated 330 ml-glass sampling bottles with Viton O-rings stopcocks (*Louwers Hapert*) that were treated with 100 μl saturated $HgCl_2$ solution (7 mg $HgCl_2$) before sampling (Emerson et al., 1995). Samples were carefully drawn into the vessel by overflowing the side-neck, to avoid atmospheric oxygen contamination, filling the vessel up to about 55 % by volume (range: 40 to 69 %), slightly below the optimum fill level of

85 % that is required to extract the maximum fraction of O_2 (Appendix A). Samples were prevented from leaking by filling the side-necks with water and capping (Luz et al., 2002). Within one month of the end of the cruise the gas from all samples was extracted and stored in sealed glass tubes with molecular sieves. We extracted the gas samples and removed water vapour, CO_2 and N_2 by cryogenic trapping and gas chromatography before measuring O_2/Ar and O_2 isotopologue ratios ($^{16}O^{17}O/^{16}O_2$, $^{16}O^{18}O/^{16}O_2$) using a Finnigan MAT 252 isotope ratio mass spectrometer. The standard error for standard samples was 0.03 ‰ for $\delta(^{17}O)$ and 0.05 ‰ for $\delta(^{18}O)$. Our purification line was based on the method of Barkan and Luz (2003) and Abe (2008). Tests with artificial O_2/Ar mixtures showed that there was no isotopic fractionation of the gas sample during extraction and purification.

2.3 Calculation of net community production, $N(O_2/Ar)$

The O_2/Ar method is based on the similar solubility and diffusivity properties of the dissolved oxygen and argon. Only dissolved O_2 is affected by biological production and consumption processes. The relative difference between sample O_2/Ar and calculated saturation O_2/Ar ratio can therefore be used to express the magnitude of the biological O_2 supersaturation (Craig and Hayward, 1987; Kaiser et al., 2005):

$$\Delta(O_2/Ar) = [c(O_2)/c(Ar)]/[(c_{sat}(O_2)/c_{sat}(Ar)] - 1 \qquad (1)$$

where c is the dissolved gas concentration and c_{sat} is the air-saturation concentration at a certain temperature, salinity and atmospheric pressure.

$\Delta(O_2/Ar)$ reflects the biological processes affecting mixed layer oxygen concentrations (production and respiration), but is not significantly affected by physical processes such as heat and freshwater fluxes or bubble injection and exchange. In combination with estimates of gas exchange rates (usually based on wind-speed), $\Delta(O_2/Ar)$ can be used to calculate biological O_2 fluxes (F_{bio}):

$$F_{bio} = k(O_2)c_{sat}(O_2)\Delta(O_2/Ar) \qquad (2)$$

where $k(O_2)$ is the O_2 gas exchange coefficient calculated from a wind speed-based parameterisation (Nightingale et al., 2000) and $c_{sat}(O_2)$ is the oxygen in air-saturation concentration at a given seawater temperature, salinity and atmospheric pressure (García & Gordon, 1992; Hamme & Emerson, 2004).

F_{bio} can be used to estimate net community production, where the second derivative of oxygen concentration $c(O_2)$ with respect to time is 0, and the effects of horizontal

and vertical mixing on the O_2/Ar ratio are negligible (Kaiser et al., 2005). In shelf seas, these conditions are often not met, and we apply corresponding corrections for non steady-state conditions here.

For $k(O_2)$, we compared the parameterisation of Nightingale et al. (2000) to that of Wanninkhof (2014), but prefer the former because it is based on two experiments in European shelf seas and because its use was recommended for winds at intermediate speed (3.5-15 m s^{-1}), which cover the range we encountered in the Celtic Sea. However, F_{bio} calculated using the Wanninkhof (2014) parameterisation or other recent wind-speed gas-exchange parameterisations (e.g. Ho et al., 2006; Sweeney et al., 2007) would change $k(O_2)$ by <5 %, which is a negligible uncertainty. The gas exchange coefficient is scaled to the in situ Schmidt number of O_2 by multiplication with the factor $(Sc(O_2)/600)^{-0.5}$. The calculation of the Schmidt number is based on Wanninkhof (2014). We use Cross Calibrated Multi Platform (CCMP) wind speeds at 0.25° and 6 h resolution (http://www.remss.com/measurements/ccmp) for the calculation of the gas exchange velocities. A comparison of CCMP winds with anemometer measurements at the Met Office ODAS buoy positioned in the centre of the Celtic Sea showed that they agreed to within (0.2±0.2) m s^{-1}. Winds measured directly by the ship were also compared with the CCMP winds, and appeared to be (1.5±2.0) m s^{-1} higher. Ship wind measurements can be affected by the ship's hull geometry (Moat et al., 2005) and for this reason have not been used in the present analysis.

Correction for non-steady state conditions, entrainment into the mixed layer and diapycnal mixing across the base of the mixed layer

Entrainment of water from below the mixed layer and diapycnal mixing across the base of the mixed layer need to be taken into account for accurate biological oxygen production calculations (Luz & Barkan, 2000; Nicholson et al., 2012; Palevsky et al., 2016; Quay et al., 2012; Quay et al., 2010). The O_2/Ar gradient will determine if F_{bio} over- or underestimates production in the mixed layer. The contribution of vertical mixing across the base of the mixed layer (F_v) was calculated according to the following equation (see Appendix B):

$$F_v = K_z c(O_2) \frac{d\ln\frac{c(O_2)}{c(Ar)}}{dz}$$ (3)

9

where $K_z = (3\pm2) \times 10^{-5}$ m^2 s^{-1} (Osborn, 1980; Palmer et al., 2013; Simpson & Sharples, 2012) is the vertical diffusivity coefficient, $c(O_2)$ is the oxygen concentration from the CTD oxygen sensor calibrated against discrete samples analysed on board by automatic Winkler titration to a potentiometric endpoint (Culberson, 1991; Holley & Hydes, 1995), and the third term is the O_2/Ar gradient across the base of the mixed layer.

During the period of our study, no sustained increases in mixed-layer depth (entrainment) occurred (Fig. C.1, Appendix C). Entrainment events, deepening of the mixed layer ($\Delta z > 0$), make a significant contribution only two times and were calculated as in Eq. B.7, Appendix B.

According to Ruiz et al. (this issue) there were no upwelling events in this region, thus the influence of vertical advection was not explored further.

Lateral advection was not considered either since (a) its calculation requires O_2/Ar measurements in two places at the same time and (b) we did not expect to find strong currents or gradients perpendicular to the transect. Surface currents were weak at <1 km d^{-1} (0.01 m s^{-1}) during spring 2015 (M. P. Humphreys and E. Ruiz-Castillo, pers. comm., January 2017) and previous studies have shown fronts in the Celtic Sea only in waters below the mixed layer (Brown et al., 2003; Sharples et al., 2013).

Temporal non-steady state changes in the oxygen mass balance are taken into account by the term F_{nss}:

$$F_{nss} = z_{mix}c(O_2)\frac{d\ln\frac{c(O_2)}{c(Ar)}}{dt} \tag{4}$$

This gives the following combined equation for the calculation of $N(O_2$/Ar):

$$N(O_2/Ar) = F_{bio} + F_{nss} - F_v$$

$$= k(O_2)c_{sat}(O_2)\Delta(O_2/Ar) + c(O_2)\left[z_{mix}\frac{d\ln\frac{c(O_2)}{c(Ar)}}{dt} - K_z\frac{d\ln\frac{c(O_2)}{c(Ar)}}{dz} \right] \tag{5}$$

The mixed layer depth (z_{mix}) is typically defined using density (Kara et al., 2000). However, here we use a criterion based on the O_2 concentration gradient (Fig C.1, Appendix C), which is expected to more reliably define the depth of active mixing, which is relevant for gas exchange (Castro-Morales & Kaiser, 2012).

In order to asses if primary production values could be higher for times when z_{eu} was deeper than z_{mix}, the depth of the euphotic layer (z_{eu}) (1 % of incident light) determined from daytime CTD casts was used to assess to what extent mixed-layer production reflects the overall productive zone. The contribution of $N(O_2/Ar)$ below the mixed layer depth was calculated as $\Delta(\int c(O_2)dz) / \Delta t$ at stations A, J2, J4, J6, CCS and CS2 because these were the only stations where we had frequent repeated vertical profiles ($n = 25$).

2.4 Calculation of gross production, $G(^{17}O)$

Oxygen has three naturally occurring isotopes (Hoefs, 2004). The triple oxygen isotope ratios ($^{17}O/^{16}O$ and $^{18}O/^{16}O$) of dissolved O_2 can be used to estimate gross oxygen production in the mixed layer. Initial work used an approximated equation based on the ^{17}O excess, $\Delta(^{17}O)$ (Luz & Barkan, 2000). Here we use the improved dual-isotope approach with the following equation (Kaiser, 2011b; Kaiser & Abe, 2012):

$$G_{ss}(^{17}O) = k(O_2)c_{sat}(O_2) \frac{(1+^{17}\varepsilon)\dfrac{^{17}\delta - ^{17}\delta_{sat}}{1+^{17}\delta} - \gamma(1+^{18}\varepsilon)\dfrac{^{18}\delta - ^{18}\delta_{sat}}{1+^{18}\delta} + s(^{17}\varepsilon - \gamma^{18}\varepsilon)}{\dfrac{^{17}\delta_P - ^{17}\delta}{1+^{17}\delta} - \gamma\dfrac{^{18}\delta_P - ^{18}\delta}{1+^{18}\delta}} \quad (6)$$

where ε is the kinetic isotope fractionation during O_2 evasion ($^{18}\varepsilon = -2.095$ ‰ (Knox et al., 1992) and $^{17}\varepsilon = -1.463$ ‰ (based on a mass-dependent relationship between $^{18}O/^{16}O$ and $^{17}O/^{16}O$ fractionation with an exponent of 0.522 (Kaiser, 2011b) and δ_{sat} at the measured temperature and salinity, i.e. $^{17}\delta_{sat} = (0.373\pm0.02)$ ‰ and $^{18}\delta_{sat} = (0.695\pm0.04)$ ‰ (Luz & Barkan, 2009). $\gamma = ^{17}\varepsilon_R / ^{18}\varepsilon_R = 0.5179$ is the triple isotope fractionation coefficient during respiration. $^{17}\delta_P = -11.644$ ‰ and $^{18}\delta_P = -22.832$ ‰ are assumed as the photosynthetic end-member delta values (Kaiser, 2011a; Kaiser, 2011b; Kaiser & Abe, 2012). Prokopenko et al. (2011) proposed a similar approach to the dual-delta method of Kaiser (2011b); the only difference being that they omitted the isotopic fractionation during gas exchange (ε) and the biological O_2 supersaturation $s = \Delta(O_2/Ar)$. The dual delta method has been used by a number of authors to calculate gross production rates (Castro-Morales et al., 2013; Hamme et al., 2012; Juranek et al., 2012; Nicholson et al., 2012; Palevsky et al., 2016).

The above equation 6 is valid for steady-state conditions ($G_{ss}(^{17}O)$) (Kaiser, 2011b). Similar corrections therefore have been applied for non steady-state conditions:

diapycnal diffusion $(\text{dln}[(1+^{17}\delta)/(1+^{18}\delta)^{\gamma}]/\mathrm{d}z \neq 0)$ in all the stations and $(\text{dln}[(1+^{17}\delta)/(1+^{18}\delta)^{\gamma}]/\mathrm{d}t \neq 0)$ where there are $\Delta(^{17}O)$ gradients for the mixed layer and below the mixed layer until the euphotic zone (F_{bml}), as well as entrainment $(\text{dln}[(1+^{17}\delta)/(1+^{18}\delta)^{\gamma}]/\mathrm{d}z \neq 0)$ where $\Delta z > 0$ for the stations sampled repeatedly (Kaiser, 2011b).

2.5 Calculation of f ratio

The combination of net oxygen community production and gross oxygen production allow us to calculate the efficiency of the biological pump or f-ratio: $f(O_2) = N(O_2/Ar) / G(^{17}O)$.

To calculate net community production in carbon equivalents, $N(O_2/Ar)$ was converted using a photosynthetic quotient of 1.4: $N_C = N(O_2/Ar) / 1.4$ (Laws, 1991). Similarly, to convert $G(^{17}O)$ and to make it compatible with conventional ^{14}C-labelled 24 hour-incubations, we used $P_C(^{14}C; 24\ h) = G(^{17}O) / 2.7$ (Marra, 2002). These conversions were then used to calculate the "historic" f-ratio $f_C(\text{historic}) = N_C / P_C(^{14}C; 24\ h)$.

However, this value is not always constant. Then, for comparison we also used $G_C(^{17}O) = N(O_2/Ar) / 1.4 + [0.8G(^{17}O) - N(O_2/Ar)] / 1.1$ which uses photosynthetic quotients of 1.4 for "new" production (assumed to equal net community production) and 1.1 for "regenerated" production. The factor of 0.8 corrects for water-to-water cycling reactions such as the Mehler reaction, which produce O_2 with the oxygen isotope signature of photosynthetic O_2 and consume O_2 with ambient δ values, without associated C fixation. These conversion was then used to calculate the f-ratio in terms of carbon equivalents, i.e. $f_C(O_2) = N_C / G_C(^{17}O)$ (Hendricks et al., 2004).

3. Results

3.1 Metabolic balance

Continuous O_2/Ar measurements showed a metabolic balance corresponding to net autotrophic conditions ($\Delta(O_2/Ar) > 0$) for the whole month of April (Fig. 2), with a mean of (6±4) %. During the two days of transect from the western English Channel (50° N 2° W) to station CCS (49.4° N 8.6° W), then south to CS2 and back to CCS on 10th of April, $\Delta(O_2/Ar)$ values remained relatively constant at (1.8±1) % (Figs. 2 – transit 1 & 3a). $\Delta(O_2/Ar)$ began to increase substantially from April 11th whilst the ship remained at CCS. The highest $\Delta(O_2/Ar)$ values were recorded on 15th April (up to

12

26 %) moving south from A to CCS. The cruise track followed the same transect (51.2° N 6.1° W to 48.1° N 10° W) on two occasions (numbers 1 and 2 in figure 2) and partially a third one at the end of the cruise. The first complete transect covered pre-bloom, bloom and the bloom-peak according to the $\Delta(O_2/Ar)$ recorded values (1st - 15th April). The second (15th – 27th) and third (27th – 29th) transects recorded similar values in the inner shelf of about 12 % (Fig 2). Outside the shelf, southwest of CS2, waters were undersaturated or at lower saturation than on the shelf, presumably due to Atlantic waters with lower $\Delta(O_2/Ar)$ values mixing with shelf waters in the less strati-fied water column.
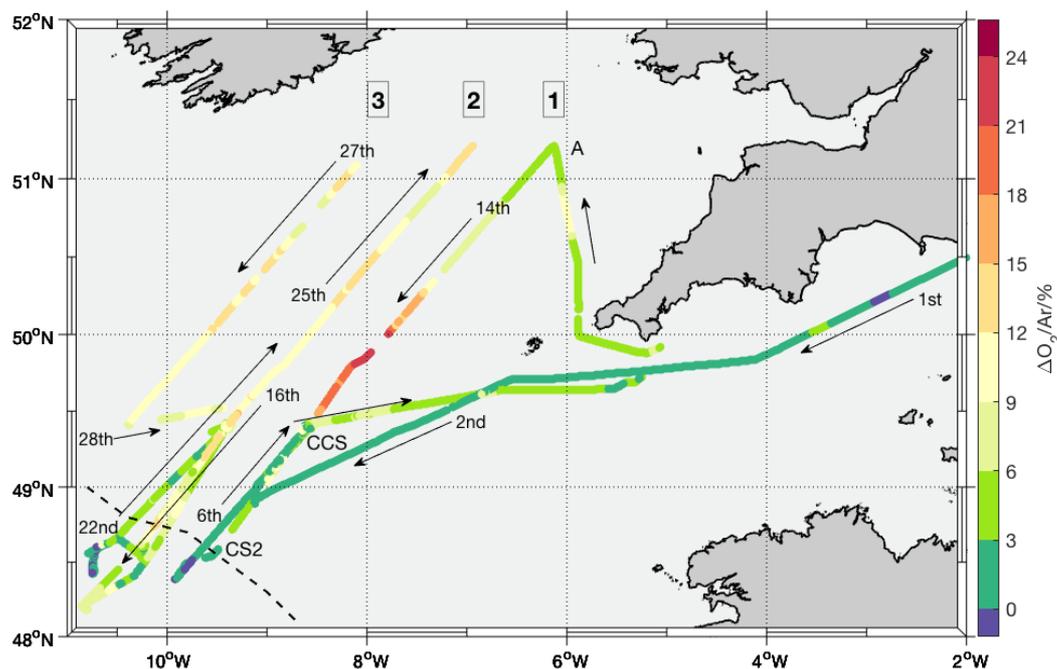

Fig. 2. $\Delta(O_2/Ar)$ along the cruise track in the Celtic Sea and English Channel. Numbers 1, 2, 3 shows the first (1st – 15th April), second (15th – 27th) and third transect (27th – 28th), respectively. For clarity, transects 2 and 3 have been displaced by 0.9 and 1.9 ° W to the west, respectively. A, CCS, CS2, indicate approximate location of the inner, central and outer stations, arrows shows direction of traveling and approxi-mate date, and dashed line indicates the shelf edge.

3.2 Biological oxygen sea-air fluxes from continuous sampling

Biological oxygen fluxes between surface waters and the atmosphere for the entire cruise were calculated from $\Delta(O_2/Ar)$ (Fig. 3a) using Eq. 2. The resulting F_{bio} values from two wind-speed gas exchange parameterisations, Wanninkhof (2014) and

Nightingale et al. (2000), are shown in Figure 3b. Both parameterisations give virtually indistinguishable results except during the strongest winds (> 9 m s^{-1}; corresponding to $k > 5$ m d^{-1}; Fig 3a). For low and intermediate wind speeds the differences in F_{bio} with different parameterisations were negligible. Mean F_{bio}(N2000) was (56±32) mmol m^{-2} d^{-1}, but was higher after 11 April when the spring bloom started. The combination of O_2 supersaturation in the surface layer during the spring bloom and stronger winds resulted in the highest F_{bio} values during spring bloom decay (Fig. 3b).
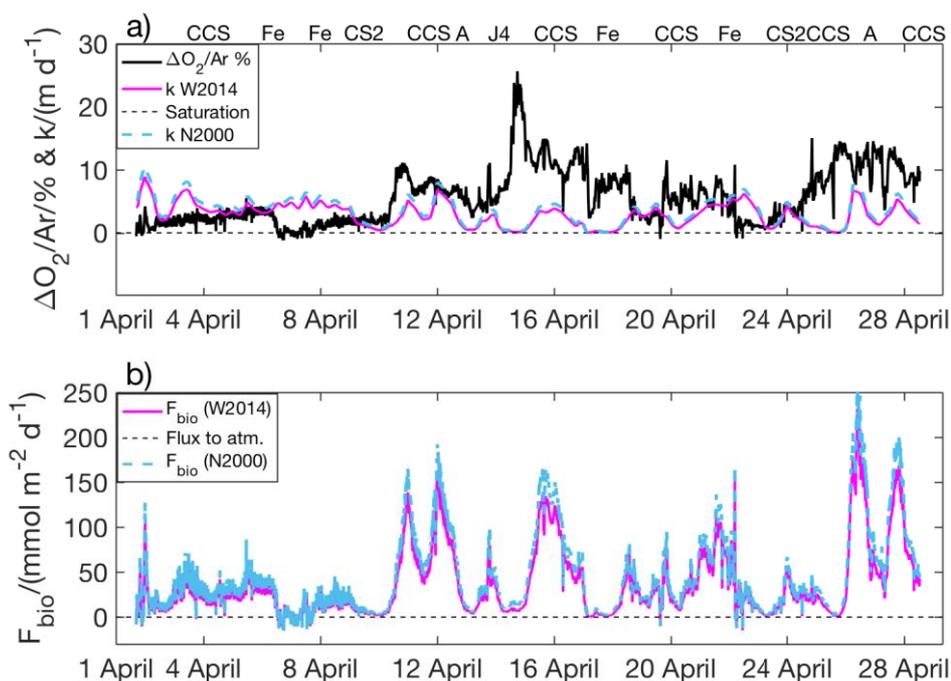

Fig. 3. (a) O_2/Ar supersaturation ($\Delta(O_2/Ar)$) from the USW during April 2015. Negative values mean undersaturation. Gas exchange coefficients based on wind speed parameterisations according to Wanninkhof (2014) shown in pink (W2014); according to Nightingale et al. (2000) in dashed blue (N2000). (b) Biological sea-to-air O_2 fluxes (F_{bio}) are >0, air-to-sea fluxes are < 0.

3.3 Net community production, diapycnal diffusion and temporal changes

To evaluate how well F_{bio} approximates net community production, we considered the influence of vertical transport due to diapycnal diffusion and temporal non-steady state.

Diapycnal diffusion

Diapycnal diffusion, F_v, was calculated as per Eq. 3 (Fig. 4) when the ship was on station and linearly interpolated over time. The mixed layer depth was generally shallow, around 20 m. F_v was generally negative throughout, which corresponds to loss of oxygen from the mixed layer to below; consequently, subtracting negative F_v values from F_{bio} result in higher $N(O_2/Ar)$ values. Values of F_v ranged from +0.5 to -10.1 mmol m^{-2} d^{-1}. The average F_v ($K_z = (3\pm2) \times 10^{-5}$ m^2 s^{-1}), -3.7 ± 2.5 mmol m^{-2} d^{-1}, accounts for about 6.7 % of F_{bio}, thus diapycnal diffusion made a small contribution to $N(O_2/Ar)$.
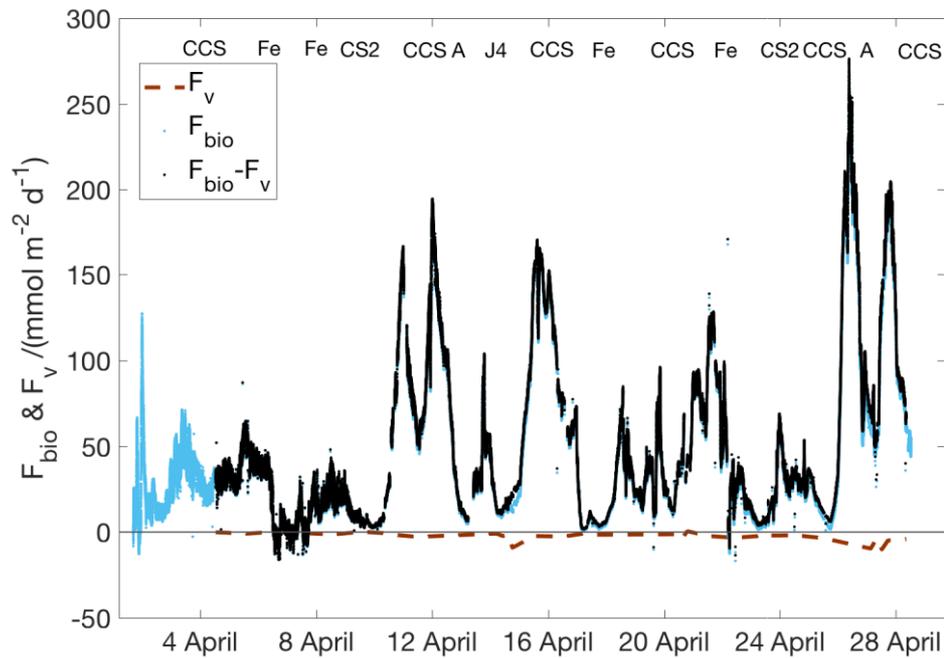

Fig. 4. Time variations in F_{bio} accounting for diapycnal diffusion. Diapycnal diffusion (F_v) calculated from oxygen based mixed layer depth (differences of 0.5 % with the near-surface concentration) in dashed brown. $F_{bio} - F_v$ in black.

Temporal non-steady state changes

The temporal change term, F_{nss}, was calculated as the change in $\Delta(O_2/Ar)$ over the time interval between repeat occupations of the transects 1 and 2 (Fig. 2 & 5), as indicated in equation 4. Transect 3 was not used for the calculation of F_{nss} as there is not significant change in $\Delta(O_2/Ar)$ in respect to transect 2. F_{nss} was mainly negative from the central to the southern part of the transect (Fig. 6), meaning a loss of oxygen with time. From 50.2° N, F_{nss} was positive, corresponding to a biological oxygen gain.

15

Overall, values of F_{nss} ranged from +61 to -56 mmol m^{-2} d^{-1}. The average F_{nss}, -2 mmol m^{-2} d^{-1}, accounted for about -3.6 % of F_{bio}. In the calculation of $N(O_2/Ar)$, F_{nss} was added to the mean $F_{bio} - F_v(O_2)$ for the main transect.
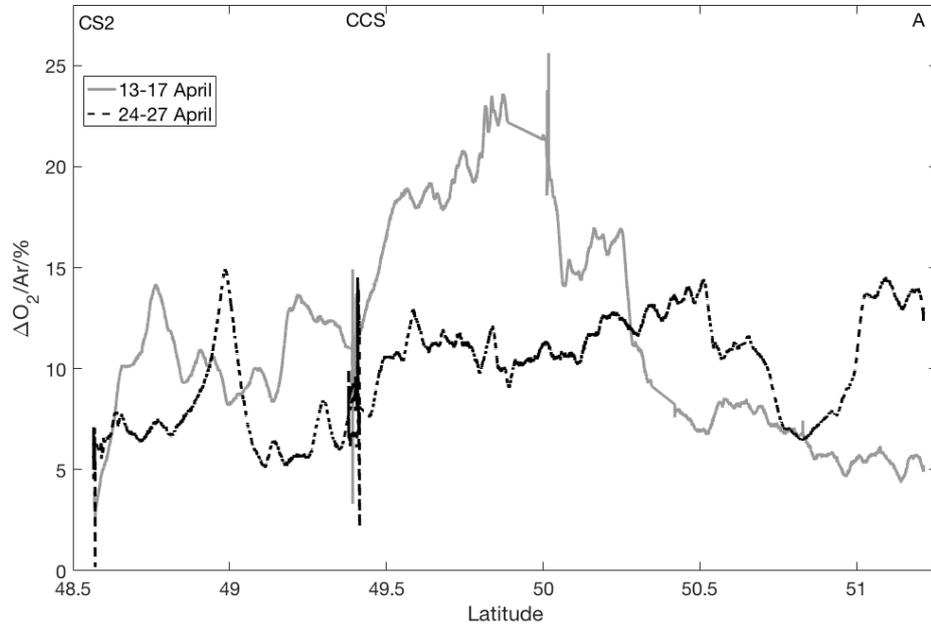

Fig. 5. $\Delta(O_2/Ar)$ time variation for the 13-17 April transect from station A to CS2 (grey line) and the 24-27 April transect from CS2 to A (dashed black) between 48.5° N and 51.5° N. The approximate locations of stations A, CCS and CS2 are also indicated on the plot.
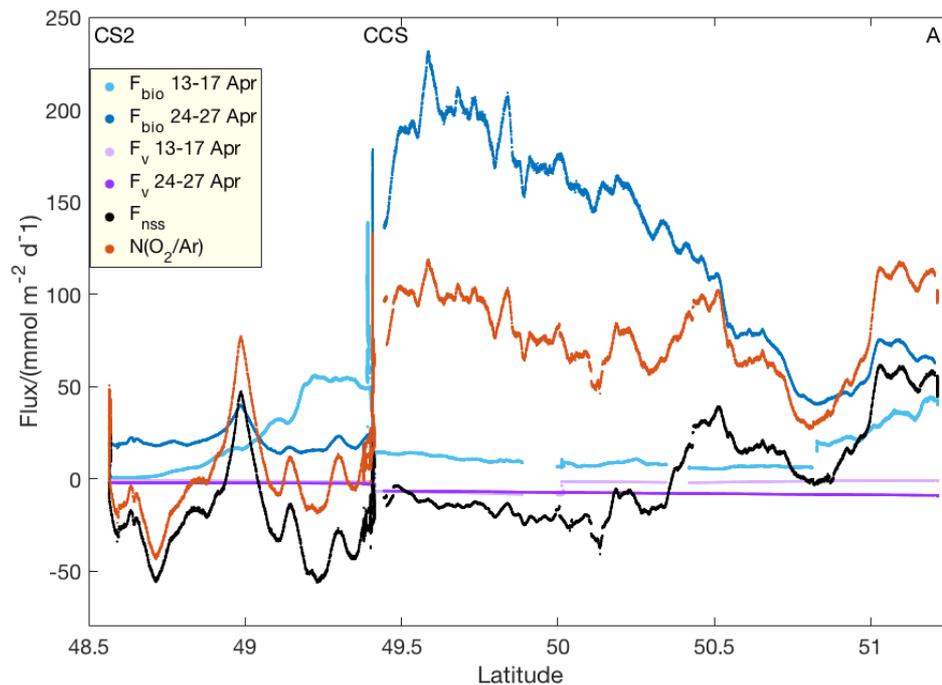

16

Fig. 6. Net community production, diapycnal diffusion and temporal non-steady state oxygen fluxes during the first transect (13 to 17 April; light blue and purple) and the second transect (24 – 27 April; dark blue and purple). F_{nss} (in black) and $N(O_2/Ar)$ (in orange) correspond to the period between first and second transect.

Net community production, $N(O_2/Ar)$, represents the combination of the biological oxygen fluxes, diapycnal diffusion and temporal changes, cf. Eq. 5. The average value was (33 ± 41) mmol m^{-2} d^{-1}, thus the Celtic Sea was net autotrophic (see Fig. 7). The highest $N(O_2/Ar)$ values were found at stations CCS and A, 133 and 117 mmol m^{-2} d^{-1} respectively (Figs. 6 & 7). However, from CCS to the CS2, the Celtic Sea appeared very patchy in its southern part with some negative $N(O_2/Ar)$ values, accordingly this section was net heterotrophic. Therefore, our $N(O_2/Ar)$ calculations show that at high spatial resolution the Celtic Sea is heterogeneous during the spring bloom.
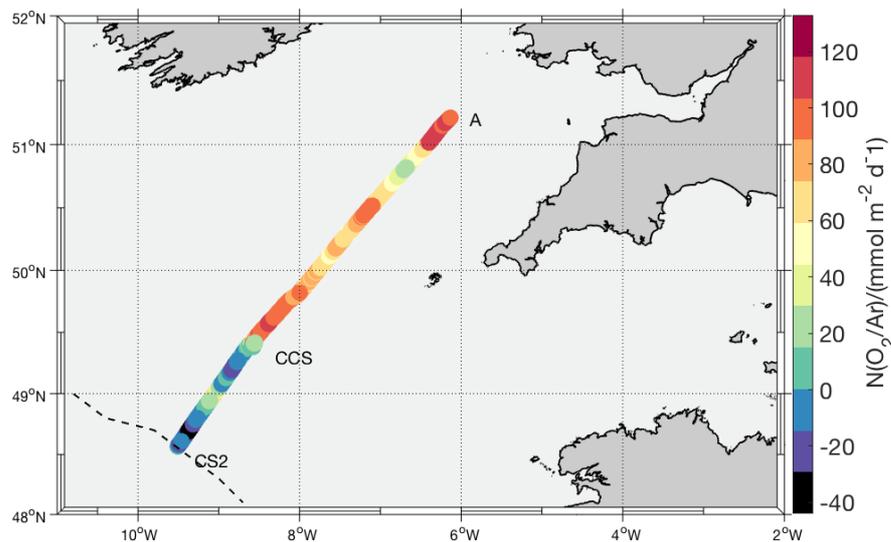
Fig. 7. Zonal variations of net community oxygen production ($N(O_2/Ar)$) along the Celtic Sea as a composite of first and second transect, calculated using equation 5. The approximate location of the main stations A, CCS and CS2 is also indicated on the plot. Dashed line indicates the shelf edge.

3.4 Net community production, gross production and *f* ratio from discrete samples

Gross oxygen production is calculated from *in situ* discrete CTD samples and calculated using the dual-delta method (Eq. 6). $G(^{17}O)$ also shows that the Celtic Sea appeared very patchy with an average value of 225 mmol m^{-2} d^{-1}, ranging from 0 to 424

mmol m^{-2} d^{-1} (Fig. 8). Values of $F_v(^{17}O)$ ranged from +20 to -21 mmol m^{-2} d^{-1}. The average $F_v(^{17}O)$, -5.4 mmol m^{-2} d^{-1}, accounts for about 2.6 % of G in steady state, thus diapycnal diffusion made small contribution to $G(^{17}O)$. $F_{nss}(^{17}O)$ was mainly negative during the peak of the bloom, meaning a loss of photosynthetic oxygen over time. Before and after the peak of the bloom F_{nss} was positive, corresponding to a biological oxygen gain. Overall, values of F_{nss} ranged from +217 to -201 mmol m^{-2} d^{-1}. The average F_{nss}, 36.4 mmol m^{-2} d^{-1} or 18 % of G in steady state, made more significant contribution to $G(^{17}O)$. Euphotic zone deeper than the mixed layer depth occurred seven times. Only in two of them, before the peak of the bloom, F_{bml} was positive (63 and 22 mmol m^{-2} d^{-1}), meaning gross production below the mixed layer. Entrainment made an important contribution (291 mmol m^{-2} d^{-1}) only at CCS at the end of the sampling period.
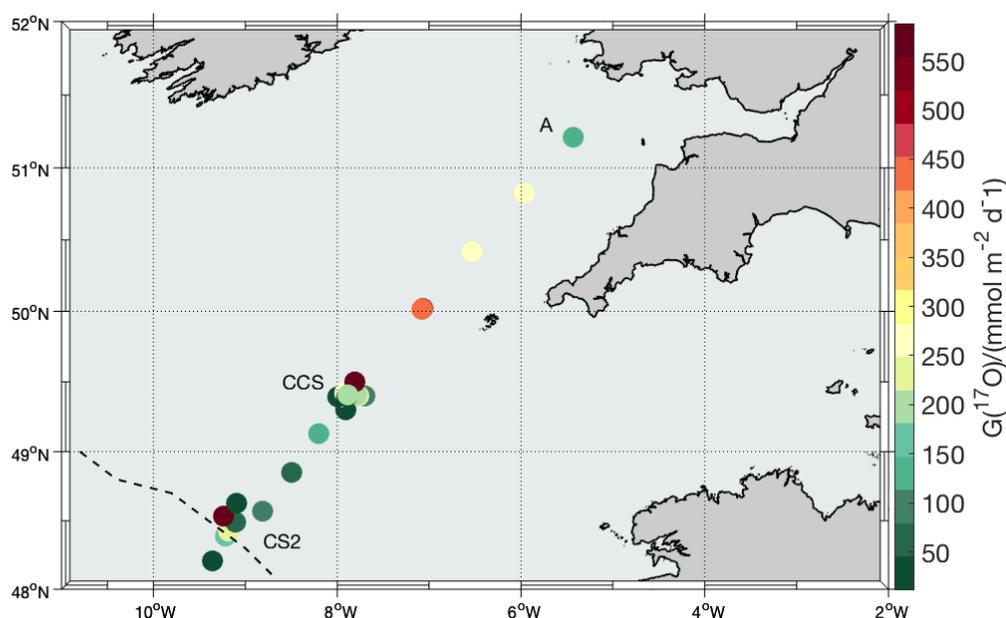
Fig. 8. Zonal variations of gross oxygen production ($G(^{17}O)$) based on oxygen triple isotopic measurements from CTD along the Celtic Sea and calculated using equation 6. The approximate location of the main stations A, CCS and CS2 is also indicated on the plot. Dashed line indicates the shelf edge.

From the same discrete samples, $N(O_2/Ar)$ values were obtained. These samples has been corrected in the same way as $G(^{17}O)$ measurements. The average of F_v, F_{nss}, F_{bml}, and F_e was -1, 19, 3 and 8 mmol m^{-2} d^{-1} respectively (Table 1). Using F_v, F_{nss}, F_{bml}, and F_e terms for the calculation of $N(O_2/Ar)$ and $G(^{17}O)$ we found a correlation

($R^2 = 0.22$, $n = 11$, $p < 0.001$). The $f(O_2)$-ratio was determined by linear regression of $N(O_2/Ar)$ against $G(^{17}O)$ as (0.14 ± 0.09) for the stations that we sampled multiple times, therefore, not including two of the station on shelf neither the station out of shelf. To calculate $f(O_2)$ for the entire sampled area (on and off shelf) and from the beginning to the end of the sampled period, we used a more simple mass balance approach by using the F_v as non steady-state term only. We found a good correlation between $N(O_2/Ar)$ and $G(^{17}O)$ values ($R^2 = 0.58$, $n = 33$, $p < 0.001$). $f(O_2)$-ratio for the entire sampled area was (0.18 ± 0.03) (Fig. 9), similar to the more complex approach value of (0.14 ± 0.09). However, interestingly $f(O_2)$ yielded different correlations and slopes for samples taken on or off the shelf. The $f(O_2)$ ratio slope corresponding to the samples off the shelf was notably lower $(0.07\pm0.02, R^2 = 0.69)$ than from the samples on the shelf $(0.25\pm0.02, R^2 = 0.91)$ regardless of the time. In terms of carbon equivalents and for comparison with historical data (i.e. the ratio $N_C / P_C(^{14}C; 24 \text{ h})$, see Method section 2.5), $f_C(\text{historic})$ for off and on the shelf was 0.13 and 0.49, respectively. $f_C(O_2)$ in terms of carbon according to Hendricks et al. (2004) (i.e. the ratio $N_C / G_C(^{17}O)$, see Method section 2.5), for off and on the shelf was 0.06 and 0.25 respectively.
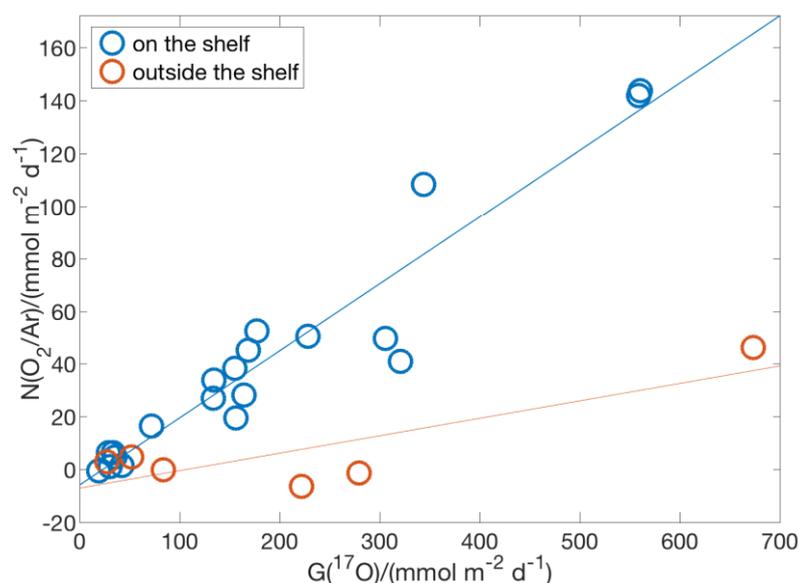

Fig. 9. Net oxygen community production ($N(O_2/Ar)$) vs. gross oxygen production ($G(^{17}O)$) from CTD water samples in the Celtic Sea. A linear regression for samples on the shelf gives $N(O_2/Ar) = (0.25\pm0.02) G(^{17}O) - (5.7\pm4.5)$ mmol m^{-2} d^{-1} (blue circles and line; $R^2 = 0.91$). The regression for samples from outside the shelf gives

$N(O_2/Ar) = (0.07\pm0.02)\ G(^{17}O) - (6.9\pm6.9)$ mmol m^{-2} d^{-1} (orange circles and line; R^2 = 0.69).

Table 1. Net community production at steady-state or biological O_2 fluxes (F_{bio}), gross production at steady-state ($G_{ss}(^{17}O)$), diapycnal diffusion (F_v) and $f(O_2)$ for all stations visited. Temporal non-steady state term (F_{nss}), production below the mixed layer (F_{bml}) and entrainment (F_e) for the stations visited repeatedly (units: mmol m^{-2} d^{-1} of O_2 equivalents). Stations on the first column as per order sampled. Hypens mean there is no sample.

	F_{bio}	F_v	F_{nss}	F_{bml}	F_e	$G_{ss}(^{17}O)$	F_v	F_{nss}	F_{bml}	F_e	$f(O_2)$
CCS	20	0	78	13	-4.9	153	-2	86	13	2	0.1
CCS	37	-1	40	0		-	-	-	-		-
Fe08	-6	0				225	3				0.0
Fe11	-2	-1				277	-2				0.0
Fe14	0	0				65	-18				0.0
CS2	1	-1	18	0		41	-1	214	0		0.0
O4	16	0				75	4				0.2
O2	43	-2				159	-10				0.3
CCS	35	-3	58	10		152	-2	217	10		0.2
A	28	0	15	0		164	0	113	0		0.2
J2	5	0	4	0		32	-3	40	0		0.1
J4	6	0	18	0	0	27	-6	19	0	1	0.2
J6	0	1	29	0	-1	16	-3	-29	0	5	0.0
J6	138	-4				541	-18				0.3
CCS	64	-2	-35	-5		227	-4	-72	-10		0.3
CCS	5	-1			0	32	-4			0	0.2
CS2	1	0	13	3		21	-9	-69	3		0.0
Fe01	4	1				22	-5				0.1
CCS	19	-1	19	5		120	-3	81	-42		0.2
CCS	27	-1				128	-2				0.2
CCS	34	3				276	-17				0.1
CCS	70	8				345	-14				0.2
CCS	52	5				264	20				0.2
CCS	126	-2				675	-11				0.2
Fe17	45	-2				664	-9				0.1
Fe20	6	2				67	15				0.1
CS2	27	0				129	-5				0.2
CCS	4	-3	-34	7	48	20	-9	-201	7	291	0.2
A	45	-7				157	-21				0.3
J2	39	-2				307	-13				0.1
J4	101	-7				335	-9				0.3
J6	140	-4				550	-11				0.3

CCS	48	-3		221	-7	0.2

4. Discussion

Our MIMS-based approach has shown that within a relatively short period during the spring bloom, $\Delta(O_2/Ar)$ can increase very rapidly (e.g. 15 % in less than 6 hours). In the following, we discuss the dynamic changes during the spring bloom period, to what extent the steady state assumption can be used when relating biological oxygen air-sea fluxes to net community production and what the implications of the observed changes in $f(O_2)$ are for organic carbon export.

4.1 Evolution of the spring bloom

Low winds 10th-11th April on the outer part of the shelf (between the shelf edge (CS2) and CCS) led to z_{mix} shoaling above the euphotic depth (z_{eu}), which led to an increase in the biological oxygen production, $\Delta(O_2/Ar)$ (Fig 3a & Fig C.1, Appendix C). During transitting (13th- 16th) we covered the inner part of the shelf (stations A to CCS) when lower wind speed seemed to trigger the highest $\Delta(O_2/Ar)$ values of the spring bloom on the 15th. This was also considered the peak of the spring bloom by independent primary production experiments using ^{14}C uptake (Poulton et al. in this issue, García-Martín et al. in this issue). This period is also coincident with the maximum in Chl-*a* as observed by satellite (Fig C.2, Appendix C) On this occasion z_{mix} was very shallow and generally coincident with z_{eu}. After two days in CCS, we continued the transect in the direction of CS2. Net community production decreased further south with values of oxygen supersaturation close to 0 % or below on some areas out of the shelf. This could be due to the fact that the water column tends to stratify later at the shelf edge than on the shelf (Joint et al., 2001) and therefore mixing with the deeper Atlantic undersaturated waters (Nolan & O'Boyle, 2011). Although, this could be due to the timing of the bloom being later off of the shelf than on shelf, the chlorophyll satellite observations of the last week of the cruise does not show the same high values of chlorophyll off shelf than in the previous two weeks on shelf. Nevertheless, we cannot assume that other regions would not exhibit a peak in biological activity after our period of sampling.

Back at CCS, average $\Delta(O_2/Ar)$ remained almost constant on 20 and 21 April. This suggests that spatial variability is greater than temporal variability after the peak of the bloom (Fig 3a). From the 25th to the end of the sampling period on 29th of April,

21

we passed the same transect on the inner shelf twice. During this time, $\Delta(O_2/Ar)$ was quite constant. In general, higher values occurred on the inner shelf and lower ones on the outer shelf. The differences in $\Delta(O_2/Ar)$ for stations occupied repeatedly shows that the shelf sea is a dynamic and heterogeneous system. To assess if it is due to: a) the timing of the bloom varying across the study region and that the cruise captured different phases of the bloom in different areas, or b) if the spring bloom is really more intense in some areas we used chlorophyll maps at different times of the bloom (Fig C.2, Appendix C). Based on it, we can say that the later is true, and the Celtic Sea is very heterogeneous, and that the short-lived peak in biological oxygen super-saturation (e.g. an increase of 15 % in $\Delta(O_2/Ar)$ over less than 6 hours and a distance of 20 km) was captured during the spring bloom. This shows the importance of high-resolution techniques for biological production measurements under the studied seasonal and geographical conditions.

What triggered the spring bloom should be a combination of light, water column stratification and the availability of nutrients (Simpson & Sharples, 2012). As expected prior to the spring bloom, surface nutrient concentrations were at their annual peak (Ruiz-Castillo et al. in this issue). The water column became more stratified after the 10th of April due to lower winds (Fig. 3a), which probably have triggered the beginning of the spring bloom. The peak of the bloom occurred around the 15th. From the beginning of the bloom, the water column was well stratified. But from the 14th to the 16th, the mixed layer shoaled in response to weaker winds Moreover, z_{eu} was coincident with z_{mix} (Fig C.1, Appendix C). This condition of shallower mixed layer, with nutrients and light available may have triggered the peak values of the spring bloom. After the peak of the bloom, $\Delta(O_2/Ar)$ showed oversaturation, to a lesser degree, until the end of the cruise. Only on the last day, a decrease in $\Delta(O_2/Ar)$ oversaturation was recorded (Fig. 2 & Fig. 3a). That could be an early observations of the decay of the bloom, perhaps triggered by nutrient depletion, grazing or coagulation (Tiselius & Kuylenstierna, 1996).

4.2 Biological production in the Celtic Sea

For comparison, we converted previous studies that measured biological production in the Celtic Sea during springtime to O_2 equivalents (Table 2). However, different techniques do not measure the same quantity even if they all measure "biological production", making the comparison between techniques very difficult (Juranek & Quay,

2013). Incubation times can vary from one study to another, leading to recycling of ^{14}C, and dissolved organic carbon fluxes are often ignored. For example, ^{14}C with incubation time of 24 hours approximates to net primary production (gross primary production minus autotrophic respiration), while incubation times between 2 and 6 hours are considered to get results closer to gross primary production.

With these caveats in mind, we compared our gross and net values with previous studies in the Celtic Sea spring bloom (Table 2). Our production estimates are within the range of previous studies, mainly because the range of previous studies is very large. Studies conducted in summer in the Celtic Sea show $P_C(^{14}$C, 2–4 h) between 38 to 88 mmol m^{-2} d^{-1} (Hickman et al., 2012) and $P_C(^{14}$C; 24 h) from 63 to 180 mmol m^{-2} d^{-1} (Poulton et al., 2014). Incubation experiments gave spring bloom $P_C(^{13}$C; 24 h) values of 31 to 310 mmol m^{-2} d^{-1} in a relatively close North Atlantic temperate shelf sea area (Daniels et al., 2015), showing that our values are in the same order of magnitude of adjacent spring bloom events.

We compared our values with other studies that assumed steady state or integrated over the euphotic zone instead of the mixed layer. To asses for the contribution of production below the mixed layer, we calculated its contribution for times when z_{eu} was deeper than z_{mix}, but calculation of production below the mixed layer did not show a significant contribution to our $N(O_2/Ar)$ estimation (see section 2.3). To test for the difference between steady and non-steady state with high spatio-temporal resolution measurements, we calculated the diapycnal diffusion and the temporal changes. In general, diapycnal diffusion (F_v) was less than 4 mmol m^{-2} d^{-1}, and the temporal non-steady state change flux F_{nss} was 2 mmol m^{-2} d^{-1}. This is a small contribution to the F_{bio}; then, the steady state assumption could be valid to represent the net community production when considering the Celtic Sea transect as a whole and assuming we are always sampling the same water mass. However, the magnitude of F_{nss} varies from positive to negatives values (+61 to -56 mmol m^{-2} d^{-}1). This suggests that although the time resolution is very fine (every 10 s), the time resolution inherent to cruise track (time between transect 1 and 2) may not be enough to fully capture all of the changes in this dynamic system. From station J6 to the shelf edge the contribution of F_{nss} is mainly negative, greatly contributing to the heterotrophic conditions, while in the inner area of the shelf, from station A to J4 (51.5º N to 50.5º N), F_{bio} was 41 mmol m^{-2} d^{-1}, but with the contribution of F_v and F_{nss} to the final $N(O_2/Ar)$ it is 74 mmol m^{-2} d^{-1} and clearly showing this area as net autotrophic. Therefore, the steady

state assumption could underestimate daily primary production in the northern Celtic Sea by up to 55 %.

Table 2. Summary of previous results on biological production during the Celtic Sea spring bloom in comparison to the present study (units: mmol m^{-2} d^{-1} of O$_2$ equivalents). Different methods are shown in brackets. *G* stands for gross production; *P* for primary production, which is expected to be closer to *N* for 24 h. *N* stands for net community production.

References	$G(^{17}O)$	$G(^{18}O)$	$G(O_2)$	$P(^{14}C\ 24\ h)$	$N(O_2)$	$N(O_2/Ar)$
Present study	225±115					33±41
(Robinson et al., 2009)	-	58-2400	37-840	22-496	16-760	
(Joint et al., 2001; Rees et al., 1999)				168		
(Joint, 1986)				11-91		

4.3 Carbon export efficiency of the shelf sea during the spring bloom

During winter, nutrients in the mixed layer are used incompletely. Primary production fuelled by nitrate is called new production (Eppley & Peterson, 1979). The ratio of new production to total production is called *f* ratio, which, indicates the efficiency of the biological pump. Many factors can affect the efficiency of the biological pump: the structure of the plankton community, zooplankton vertical migration, phytoplankton size and taxa, and physical forcing of surface waters (Lutz et al., 2007).The combination of $N(O_2/Ar)$ and $G(^{17}O)$ shows the portion that had not been used for respiration and therefore the proportion that is available for export in O$_2$ terms (Laws et al., 2000).

Our samples show two different $f(O_2)$ ratios, with values much higher on the shelf sea than off the shelf. This indicates that off shelf the majority of the organic matter gets recycled in the mixed layer likely due to either, or a combination of, physical or biological processes like a community shift: increase in grazing pressure, smaller autotrophic cell community, larger representation of bacterial heterotrophic activity (Haskell et al., 2017; Rees et al., 1999). $f(O_2)$ ratios were 0.18±0.03 for the whole Celtic Sea and 0.25±0.02 on shelf. It is in agreement with biogeographic controls of transfer efficiency suggested in the global forecast of annual export (Lutz et al., 2007)

and values found in autotrophic areas of the Southern Ocean (Reuer et al., 2007). Slightly higher values (0.35±0.06) has been found during the spring bloom in the subpolar N. Atlantic (Quay et al., 2012) and in the N. Pacific coast ($\sim$ 0.50) (Haskell et al., 2017). Robinson et al. (2009) measured plankton production in the Celtic Sea with different incubation techniques in April 2002. Although their experiment doesn't include $f(O_2)$ ratio estimations, we calculated it from their Table 2 for comparison ($G(O_2)$ / $NCP(O_2)$ = 0.37±0.07), where production values were not obtained from triple oxygen isotopes but from oxygen evolution from incubations. Our $f(O_2)$ ratio is still higher than the most globally observed values of 0.10 to 0.20 (Juranek & Quay, 2013).

Some studies tried to find GOP (gross oxygen production) : G_C (gross carbon production; 3 – 6 h ^{14}C incubation) ratio that would allow to scale between the two techniques, but the reported values typically vary from 1.7 to 7.6 (Juranek & Quay, 2013; Luz et al., 2002; Munro et al., 2013). Recently, an experiment that compare $G(^{17}O)$: G_C ratio found a value of 1.2±1.1 which they conclude is not a definitive value and further studies are needed (Jurikova et al., 2016). With this caveats on mind, we followed Hendricks et al. (2004) to convert $G(^{17}O)$ in G_C and Laws (1991) to convert $N(O_2/Ar)$ to N_C using the photosynthetic quotient of 1.4. Our average $f_C(O_2)$ ratios (0.25±0.02) for the on shelf are comparable with average $f_C(O_2)$ ratios found by Prokopenko et al. (2011) in the spring bloom on the Bering Sea shelf. In addition, to make our values comparable to the more common f_C(historic) ratio, we divided our $G(^{17}O)$ by 2.7 (Marra, 2002) in order to convert our values to ^{14}C production $P_C(^{14}C$; 24 h). This robust relationship has been widely used for comparison with historical ^{14}C and satellite-based estimates (see Juranek and Quay (2013) for more extensive discussion) and still been in use (e.g. Palevsky et al. (2016)). To convert $N(O_2/Ar)$ to N_C we still using the photosynthetic quotient of 1.4 (Laws, 1991). Here, we study f in terms of carbon, as f_C(historic) = N_C / $P_C(^{14}C$; 24 h) represents the probability of using carbon for new production and therefore, an approximation of total primary production that is available for carbon export, whereas $1 - f$ would be the fraction of carbon used for regenerated or recycled production (Eppley & Peterson, 1979). Importantly, new production requires net inorganic carbon uptake while regenerated production does not. Our f_C(historic) ratios were 0.34±0.06 for the whole Celtic Sea. These are not the highest values recorded (Laws et al., 2000), but still higher than val-

ues found in open ocean, e.g. the equatorial Pacific (0.12 ±0.12) (Hendricks et al., 2005) or the global average of 0.20 (Laws et al., 2000).

Only two studies calculated f ratios in the Celtic Sea, specifically in the shelf edge, during the spring bloom: Rees et al. (1999) and Joint et al. (2001); they calculated f ratios of 0.8 from nitrate assimilation for samples close to the shelf edge. This values are much higher than those found in our study. This discrepancies with nitrate f ratios has been also found before (Hendricks et al., 2004). Moreover, we think that a comparison is complicated here because we would need a conversion factor C : N, but Rees et al. (1999) found highly variable C : N ratios (2.5 − 9) in their study. Therefore, converting nitrate assimilation f ratios to C or O_2 f ratios, will not give an appropriate comparison with our study.

Large microphytoplankton cells (20-200 μm) that are typical of the spring bloom are associated with higher f ratios (Tremblay et al., 1997). However, the phytoplankton community found on during the spring bloom was dominated by nanoplankton (2-20 μm) (Hickman et al. this issue), which thus may explain the lower values found in this study. Rees and Joint studies found that the spring bloom was dominated by large cells and higher f ratios when larger phytoplankton dominated the assemblage. In addition, experiments had demonstrated that phytoplankton communities dominated by small cells are more sensitive to changes in carbon concentrations (Richier et al., 2014), and the shift to smaller size-cell population, reduce the export efficiency, which could indicate an effect of climate change (Palevsky et al., 2016).

Compared to the on-shelf values, the f_C(historic) values off the shelf seems implicate three times less particulate organic carbon (POC) export than the shelf edge.

On average, our f_C(historic) ratios suggest that about 35 % of the total production is available for export and 65 % for remineralisation. It is in good agreement with annual global estimation of coastal margin carbon sequestration (Muller-Karger, 2005), because although our study does not represent annual carbon export, the spring bloom is typically the most productive season. To calculate annual carbon export requires further studies during other seasons (Palevsky et al., 2016), which will be presented in a follow-on paper.

Therefore, our f ratio is comparable, albeit sometimes slightly lower than those reported previously in other shelves, but higher than the global average, indicating that the Celtic Sea is indeed a highly productive region of the northwest European Shelf.

5. Conclusions

This is one of the first data sets of net community (N) and gross production (G) rates during a Celtic Sea spring bloom at high resolution. Our results apply to the mixed layer and below up to the euphotic zone.

We find net community production rates based on continuous membrane-inlet mass spectrometry measurements of oxygen-to-argon ratios, $N(O_2/Ar)$, of up to 144 mmol m^{-2} d^{-1} in April 2015, with an average of (33 ± 41) mmol m^{-2} d^{-1}. Biological air-to-sea oxygen fluxes (F_{bio}) were the dominant term in the $N(O_2/Ar)$ calculation. The diapycnal diffusion term (F_v) was negligibly small (< 4 mmol m^{-2} d^{-1}). The disequilibrium term (F_{nss}) contributed between -50 and $+50$ mmol m^{-2} d^{-1} at specific locations, but had a negligible effect when considering the Celtic Sea as a whole. In other words, for measurement of net community production at high spatial resolution in dynamic shelf-sea environments, good temporal resolution and repeat occupations of transects are required. The assumption of steady state (i.e. assuming $N(O_2/Ar) = F_{bio}$) may lead to errors of 50 % or more. In turn, when integrating over larger areas, F_{bio} may present a faithful representation of the metabolic balance of the Celtic Sea as a whole.

Gross production rates based on oxygen triple isotopologues in discrete samples, $G(^{17}O)$, were up to 424 mmol m^{-2} d^{-1} and (225 ± 115) mmol m^{-2} d^{-1} on average. Calculating net community production just for these discrete samples gave an average of $N(O_2/Ar) = (55\pm34)$ mmol m^{-2} d^{-1}. $f(O_2)$ ratio for the entire shelf was 0.18 ± 0.03, or $f_C(historic) = 0.34\pm0.06$ in carbon equivalents. $f(C)$ ratio is more than four times higher on the shelf than on the shelf edge. The average of nearly 0.34 for the Celtic Sea is expected to lead to a large organic carbon export flux.

The observed heterogeneity in the continuous $N(O_2/Ar)$ estimates as well as the variability of discrete $G(^{17}O)$ values along the cruise transect demonstrate the virtue of high-resolution techniques. Our results could help improve the validation of remote sensing algorithms and ecosystem models.

Appendix A: Optimum headspace for extraction of gases from water

To get the best possible precision during isotope ratio mass spectrometric analyses, it is important to maximise the amount of O_2 available for measurement. For a fixed sample bottle volume (V), the larger the water fill volume (V_W), the more O_2 is potentially available for analysis. However, a larger water fill volume reduces the headspace volume (V_A) and since only the gas in the headspace is used for our analyses, this reduces the fraction of gas in the sample available for measurement. The trade-off between these two constraints results in an optimum headspace fraction ($\eta = V_A / V$) that is solely determined by the solubility of O_2, as shown in the following.

To determine the optimum headspace fraction η, we consider the mass balance between headspace and water after equilibration as described by the equation

$$V_A c_A + \alpha V_W c_A = V_W c_0 \tag{A.1}$$

where V_A and V_W are the headspace and water volume, c_A and c_0 are the O_2 concentration in the headspace and the initial water sample and $\alpha = c_W / c_A$ is the Ostwald solubility coefficient. Substituting $V_W = V - V_A$ and rearranging for the headspace concentration gives:

$$c_A = \frac{c_0 (1 - \eta)}{(1 - \alpha)\eta + \alpha} \tag{A.2}$$

To find the optimum headspace for extracting the maximum amount of O_2 from the sample, we find the maximum of the amount of O_2 in the headspace ($n_A = c_A V_A$) with respect to the headspace fraction η using

$$\frac{\partial c_A V_A}{\partial \eta} = c_0 V \frac{\partial \left[\dfrac{(1 - \eta)\eta}{(1 - \alpha)\eta + \alpha} \right]}{\partial \eta} = 0 \tag{A.3}$$

which has the solution

$$\eta = \frac{\sqrt{\alpha}}{1 + \sqrt{\alpha}} = 1 - \frac{1}{1 + \sqrt{\alpha}} \tag{A.4}$$

for $0 < \eta < 1$.

For salinity $S = 35$ and a temperature of 10 ºC, α equals 0.032 (García & Gordon, 1992), which gives $\eta = 0.15$, i.e. the bottle should be filled with water to 85 % of its capacity. For temperatures between −2 and 35 ºC, α varies between 0.022 and 0.040, which gives η values between 17 % and 13 %.

The fraction of O_2 extracted relative to the amount in the original sample is given by

$$\frac{c_A V_A}{c_0 V_W} = \frac{1}{1-\alpha+\dfrac{\alpha}{\eta}} = \frac{1}{1+\sqrt{\alpha}} \tag{A.5}$$

i.e. under optimum extraction conditions, about 85 % of the O_2 amount in the sample are available for isotope ratio mass spectrometric analysis.

The optimum extraction conditions for argon are similar to those of O_2 because both gases share similar solubility characteristics. For less soluble gases, the headspace fraction should be decreased. For more soluble gases, the headspace fraction should be increased (Fig. A1). In the latter case, the fraction of initial gas extracted is lower, but there is also more gas to work with because of the higher solubility. This could have implications for the total volume of gas needed for an accurate measurement if a single sample is used to measure multiple gases with a range of solubilities and a range of instrument detection limits.
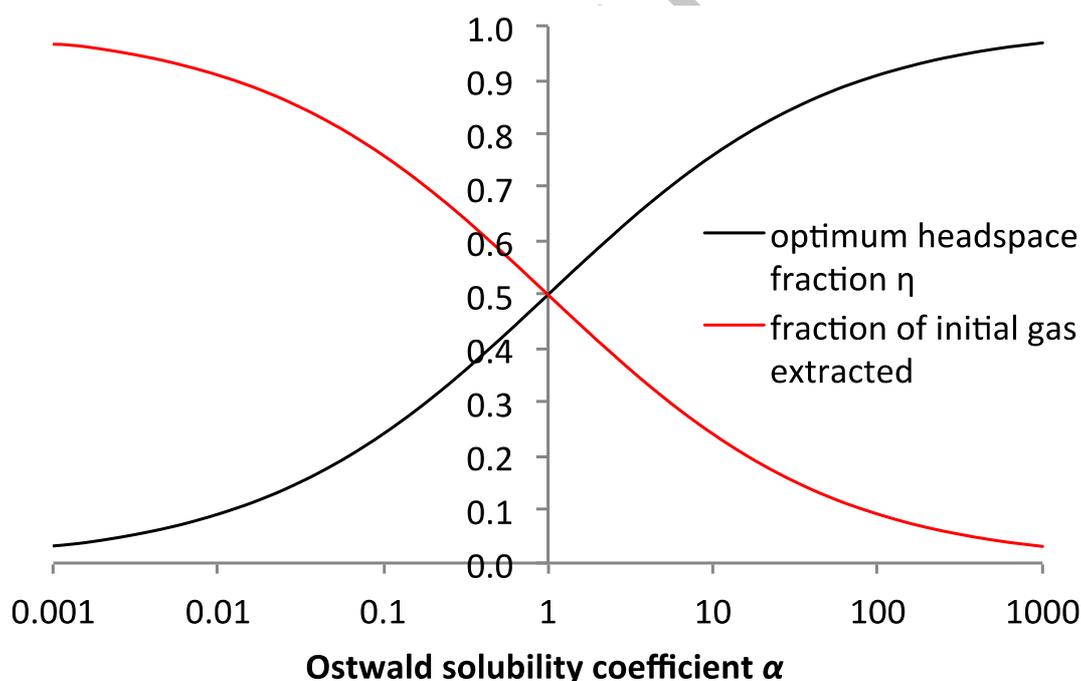

Figure A1: Optimum headspace fraction η (=V_A / V, i.e. ratio of headspace to total bottle volume) required to maximise the amount of gas in the headspace as a function of the Ostwald solubility coefficient $\alpha = c_W$ / c_A and amount fraction of initial gas extracted (= $c_A V_A$ / $c_0 V_W$).

30

Appendix B: Combined oxygen and argon mass balance in the mixed layer

We present the one-dimensional mass-balance equations for dissolved oxygen and argon in the mixed layer under the influence of net community production, air-sea gas exchange, diapycnal eddy diffusion across the base of the mixed-layer and vertical entrainment (mixed-layer deepening); last one not included in the calculations of the manuscript as no sustained increases in mixed-layer depth occurred. These equations are used as a diagnostic model to derive net community production in this study. We use the following symbols:

c, c': O_2, Ar concentrations

c_0, c_0': O_2, Ar in air saturation concentrations

c_T, c_T': O_2, Ar concentrations in the entrained water

$s = c / c_0 - 1$, $s' = c' / c_0' - 1$: O_2, Ar saturation anomalies

$\Delta = (c / c') / (c_0 / c_0') - 1$: O_2-to-Ar ratio saturation anomaly

z_{mix}: mixed-layer depth

k, k': O_2, Ar gas exchange coefficients

K_z: vertical eddy diffusion coefficient

N: net community production of O_2

The one-dimensional mixed layer mass balance for O_2 and Ar is

$$\frac{\mathrm{d}(z_{mix}c)}{\mathrm{d}t} = z_{mix}\frac{\mathrm{d}c}{\mathrm{d}t} + c\frac{\mathrm{d}z_{mix}}{\mathrm{d}t} = N - k(c - c_0) + K_z\frac{\mathrm{d}c}{\mathrm{d}z}\bigg|_{z_{mix}} + c_T\frac{\mathrm{d}z_{mix}}{\mathrm{d}t} \qquad \text{(B.1)}$$

$$\frac{\mathrm{d}(z_{mix}c')}{\mathrm{d}t} = z_{mix}\frac{\mathrm{d}c'}{\mathrm{d}t} + c'\frac{\mathrm{d}z_{mix}}{\mathrm{d}t} = -k'(c' - c_0') + K_z\frac{\mathrm{d}c'}{\mathrm{d}z}\bigg|_{z_{mix}} + c_T'\frac{\mathrm{d}z_{mix}}{\mathrm{d}t} \qquad \text{(B.2)}$$

where the eddy-diffusion terms (with K_z) include the concentration gradients at the base of the mixed layer. Using $c = c_0(1+s)$ and $c' = c_0'(1+s')$, this can be rewritten as

$$z_{mix}\frac{\mathrm{d}\ln c}{\mathrm{d}t} + \frac{\mathrm{d}z_{mix}}{\mathrm{d}t} = \frac{N}{c} - k\frac{s}{1+s} + K_z\frac{\mathrm{d}\ln c}{\mathrm{d}z}\bigg|_{z_{mix}} + \frac{c_T}{c}\frac{\mathrm{d}z_{mix}}{\mathrm{d}t} \qquad \text{(B.3)}$$

$$z_{mix}\frac{\mathrm{d}\ln c'}{\mathrm{d}t} + \frac{\mathrm{d}z_{mix}}{\mathrm{d}t} = -k'\frac{s'}{1+s'} + K_z\frac{\mathrm{d}\ln c'}{\mathrm{d}z}\bigg|_{z_{mix}} + \frac{c_T'}{c'}\frac{\mathrm{d}z_{mix}}{\mathrm{d}t} \qquad \text{(B.4)}$$

Subtracting equation B.4 from equation B.3 gives

$$z_{\text{mix}}\frac{\mathrm{d}\ln\frac{c}{c'}}{\mathrm{d}t}=\frac{N}{c}-k\frac{s}{1+s}+k'\frac{s'}{1+s'}+K_z\left.\frac{\mathrm{d}\ln\frac{c}{c'}}{\mathrm{d}z}\right|_{z_{\text{mix}}}+\left(\frac{c_{\text{T}}}{c}-\frac{c'_{\text{T}}}{c'}\right)\frac{\mathrm{d}z_{\text{mix}}}{\mathrm{d}t} \qquad (\text{B.5})$$

Using the O_2/Ar saturation anomaly $1+\varDelta=(1+s)/(1+s')$ and multiplying by c, we obtain

$$z_{\text{mix}}c\frac{\mathrm{d}\ln\frac{c}{c'}}{\mathrm{d}t}=N-kc_0\varDelta+c_0(k'-k)(s-\varDelta)+cK_z\left.\frac{\mathrm{d}\ln\frac{c}{c'}}{\mathrm{d}z}\right|_{z_{\text{mix}}}+c\left(\frac{c_{\text{T}}}{c}-\frac{c'_{\text{T}}}{c'}\right)\frac{\mathrm{d}z_{\text{mix}}}{\mathrm{d}t} \quad (\text{B.6})$$

The entrained concentration can be approximated by the concentration gradient at the base of the mixed layer and the increase in mixed-layer depth Δz_{mix}:

$$c_{\text{T}}=c+\frac{1}{2}\left.\frac{\mathrm{d}c}{\mathrm{d}z}\right|_{z_{\text{mix}}}\Delta z_{\text{mix}} \qquad (\text{B.7})$$

$\frac{1}{2}\Delta z_{\text{mix}}$ is the entrainment length scale (Castro-Morales et al., 2013; Gruber et al., 1998). This results in an entrainment term very similar to the eddy-diffusion term:

$$z_{\text{mix}}c\frac{\mathrm{d}\ln\frac{c}{c'}}{\mathrm{d}t}=N-kc_0\varDelta+c_0(k'-k)(s-\varDelta)+cK_z\left.\frac{\mathrm{d}\ln\frac{c}{c'}}{\mathrm{d}z}\right|_{z_{\text{mix}}}+\frac{1}{2}c\Delta z_{\text{mix}}\frac{\mathrm{d}z_{\text{mix}}}{\mathrm{d}t}\left.\frac{\mathrm{d}\ln\frac{c}{c'}}{\mathrm{d}z}\right|_{z_{\text{mix}}} \quad (\text{B.8})$$

Using the Schmidt numbers Sc to relate the O_2 and Ar gas exchange coefficients and rearranging for net community production N gives

$$N=kc_0\varDelta+z_{\text{mix}}c\frac{\mathrm{d}\ln\frac{c}{c'}}{\mathrm{d}t}+kc_0(s-\varDelta)\left[1-\left(\frac{Sc}{Sc'}\right)^{0.5}\right]-c\left(K_z+\frac{1}{2}\Delta z_{\text{mix}}\frac{\mathrm{d}z_{\text{mix}}}{\mathrm{d}t}\right)\left.\frac{\mathrm{d}\ln\frac{c}{c'}}{\mathrm{d}z}\right|_{z_{\text{mix}}} \quad (\text{B.9})$$

The term $1-(Sc/Sc')^{0.5}$ is about $+4.2\ \%$ (Wanninkhof (2014) Sc parameterisation) or $+4.4\ \%$ (Keeling et al. (1998) Sc parameterisation). The third term in Eq. (B.9) can therefore be neglected.

This gives the final diagnostic equation

32

$$N = kc_0\Delta + z_{mix}c\frac{\mathrm{d}\ln\frac{c}{c\phi}}{\mathrm{d}t} - cK_z\left.\frac{\mathrm{d}\ln\frac{c}{c\phi}}{\mathrm{d}z}\right|_{z_{mix}} - \frac{1}{2}c\Delta z_{mix}\frac{\mathrm{d}z_{mix}}{\mathrm{d}t}\left.\frac{\mathrm{d}\ln\frac{c}{c\phi}}{\mathrm{d}z}\right|_{z_{mix}} \tag{B.10}$$

$$= F_{bio} + F_{nss} - F_v - F_e$$

with the relation of the four terms of the equations to the quantities discussed in the manuscript: biological oxygen air-sea flux (F_{bio}), non-steady state flux (F_{nss}), diapycnal diffusion flux (F_v) and entrainment flux (F_e).

Appendix C: Mixed layer and euphotic zone depths
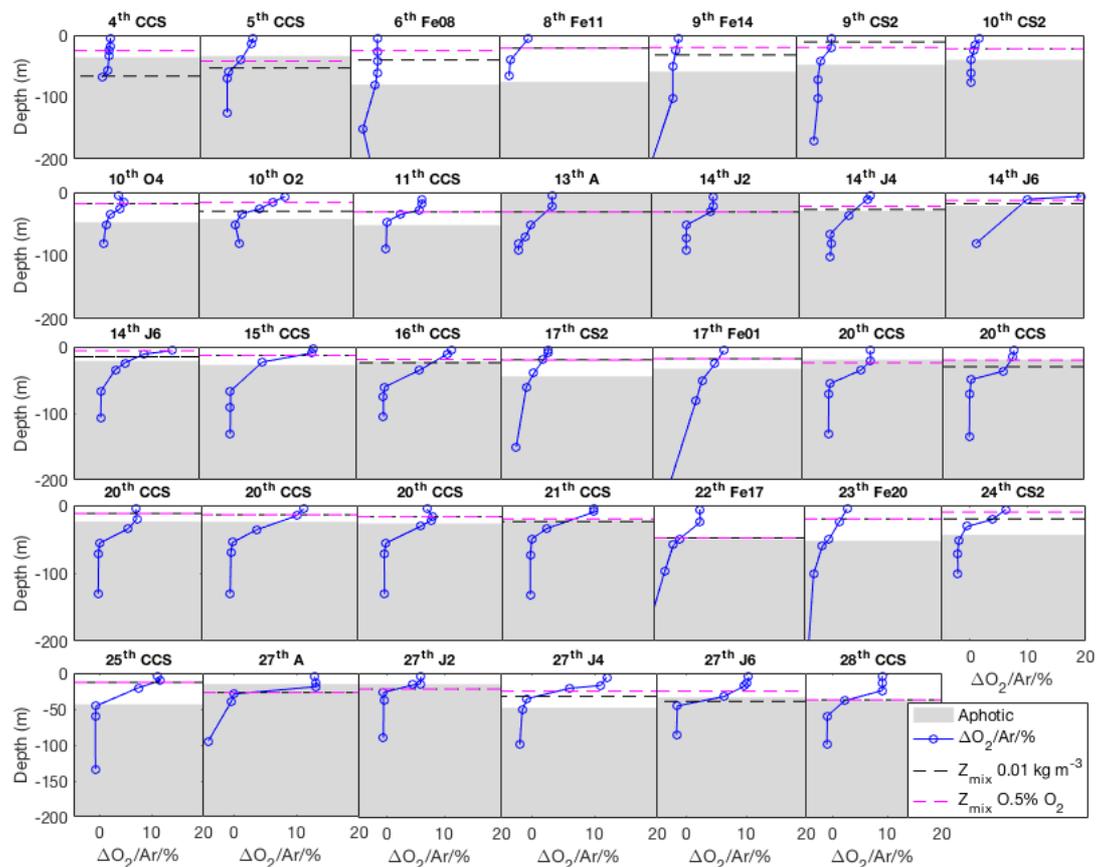

Figure C.1: $\Delta(O_2/Ar)$, mixed layer and euphotic zone from CTD casts. $\Delta(O_2/Ar)$ are plotted as blue lines. The mixed layer depth (z_{mix}) based on the change in density is in dashed black and oxygen in dashed pink. Aphotic zone (less than 1 % of incidental PAR) in shaded grey. For profiles "13th A" and "14th J2" there were no light profile measurements.

34
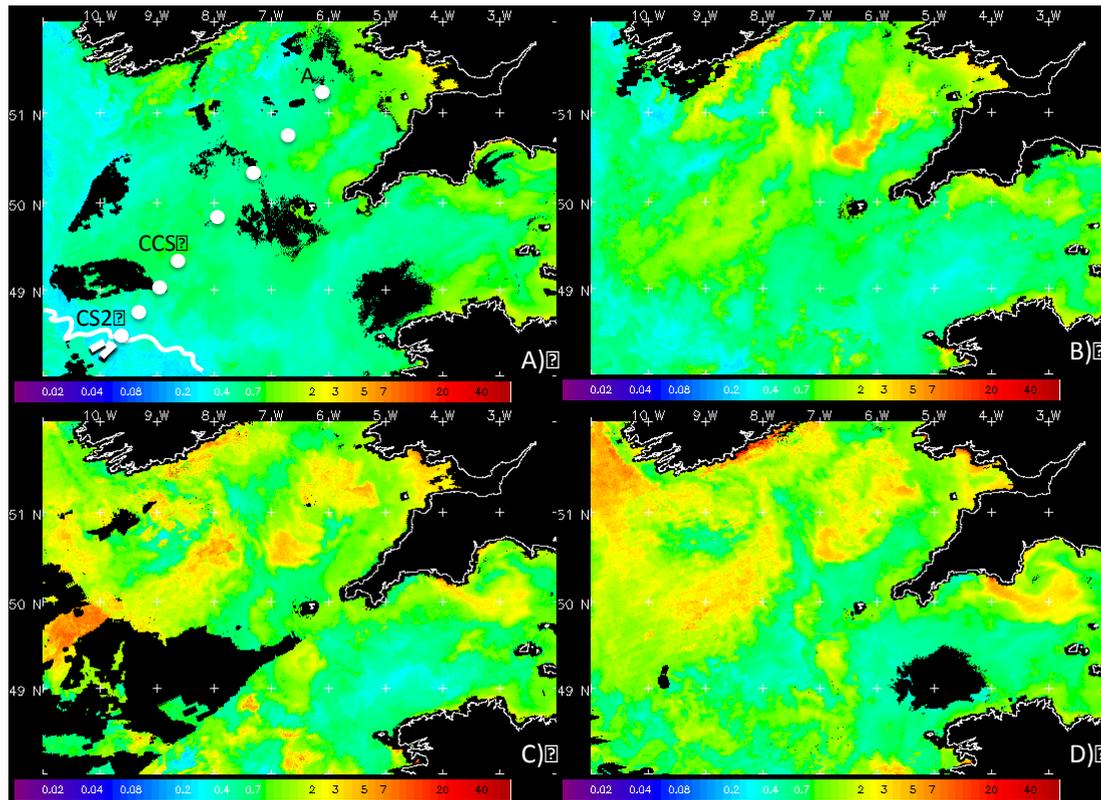
Figure C.2: Satellite images of seven days composite image from VIIRS Chlorophyll OC5 (mg m^{-3}) evolution during the spring bloom 2015. White circles, superimposed to image (A) indicate the approximate station locations (only A, CCS, and CS2 has been labelled). Straight white blocks represent multiple stations outside the shelf. The curved white line indicates the shelf-edge. (A) 1st – 7 April, (B) 8th – 14th April (C) 14 – 20th April, (D) 21 – 27 April. Images courtesy of NEODAAS.

References

Abe, O., 2008. Isotope fractionation of molecular oxygen during adsorption/desorption by molecular sieve zeolite. *Rapid Commun Mass Spectrom*, 22, 2510-2514.

Barkan, E., Luz, B., 2003. High-precision measurements of 17O/16O and 18O/16O of O2 and O2/Ar ratio in air. *Rapid Commun Mass Spectrom*, 17, 2809-2814.

Barnes, M.K., Tilstone, G.H., Suggett, D.J., Widdicombe, C.E., Bruun, J., Martinez-Vicente, V., Smyth, T.J., 2015. Temporal variability in total, micro- and nano-phytoplankton primary production at a coastal site in the Western English Channel. *Progress in Oceanography*, 137, 470-483.

Brown, J., Carrillo, L., Fernand, L., Horsburgh, K.J., Hill, A.E., Young, E.F., Medler, K.J., 2003. Observations of the physical structure and seasonal jet-like circulation of the Celtic Sea and St. George's Channel of the Irish Sea. *Continental Shelf Research*, 23, 533-561.

Campbell, J., Antoine, D., Armstrong, R., Arrigo, K., Balch, W., Barber, R., Behrenfeld, M., Bidigare, R., Bishop, J., Carr, M.-E., Esaias, W., Falkowski, P., Hoepffner, N., Iverson, R., Kiefer, D., Lohrenz, S., Marra, J., Morel, A., Ryan, J., Vedernikov, V., Waters, K., Yentsch, C., Yoder, J., 2002. Comparison of algorithms for estimating ocean primary production from surface chlorophyll, temperature, and irradiance. *Global Biogeochemical Cycles*, 16, 9-1-9-15.

Cassar, N., Barnett, B.A., Bender, M.L., Kaiser, J., Hamme, R.C., Tilbrook, B., 2009. Continuous High-Frequency Dissolved O2/Ar Measurements by Equilibrator Inlet Mass Spectrometry. *Analytical Chemistry*, 81, 1855-1864.

Castro-Morales, K., Cassar, N., Shoosmith, D.R., Kaiser, J., 2013. Biological production in the Bellingshausen Sea from oxygen-to-argon ratios and oxygen triple isotopes. *Biogeosciences*, 10, 2273-2291.

Castro-Morales, K., Kaiser, J., 2012. Using dissolved oxygen concentrations to determine mixed layer depths in the Bellingshausen Sea. *Ocean Science*, 8, 1-10.

Culberson, C.H., 1991. Dissolved oxygen. *WHP Operations and Methods*.

Daniels, C.J., Poulton, A.J., Esposito, M., Paulsen, M.L., Bellerby, R., St John, M., Martin, A.P., 2015. Phytoplankton dynamics in contrasting early stage North Atlantic spring blooms: composition, succession, and potential drivers. *Biogeosciences*, 12, 2395-2409.

Emerson, S., Quay, P.D., Stump, C., Wilbur, D., Schudlich, R., 1995. Chemical tracers of productivity and respiration in the subtropical Pacific Ocean. *Journal of Geophysical Research*, 100, 15873.

Eppley, R.W., Peterson, B.J., 1979. Particulate organic matter flux and planktonic new production in the deep ocean. *Nature*, 282, 677-680.

García, H.E., Gordon, L.I., 1992. Oxygen Solubility in Seawater: Better Fitting Equations. *Limnology and Oceanography*, 37, 1307-1312.

Gruber, N., Keeling, C.D., Stocker, T.F., 1998. Carbon-13 constraints on the seasonal inorganic carbon budget at the BATS site in the northwestern Sargasso Sea. *Deep Sea Research Part I: Oceanographic Research Papers*, 45, 673-717.

Hamme, R.C., Cassar, N., Lance, V.P., Vaillancourt, R.D., Bender, M.L., Strutton, P.G., Moore, T.S., DeGrandpre, M.D., Sabine, C.L., Ho, D.T., Hargreaves, B.R., 2012. Dissolved O2/Ar and other methods reveal rapid changes in productivity during a Lagrangian experiment in the Southern Ocean. *Journal of Geophysical Research*, 117.

Hamme, R.C., Emerson, S.R., 2004. The solubility of neon, nitrogen and argon in distilled water and seawater. *Deep Sea Research Part I: Oceanographic Research Papers*, 51, 1517-1528.

Haskell, W.Z., Prokopenko, M.G., Hammond, D.E., Stanley, R.H.R., Sandwith, Z.O., 2017. Annual cyclicity in export efficiency in the inner Southern California Bight. *Global Biogeochemical Cycles*, 31, 357-376.

Hendricks, M.B., Bender, M.L., Barnett, B.A., 2004. Net and gross O2 production in the southern ocean from measurements of biological O2 saturation and its triple isotope composition. *Deep Sea Research Part I: Oceanographic Research Papers*, 51, 1541-1561.

Hendricks, M.B., Bender, M.L., Barnett, B.A., Strutton, P., Chavez, F.P., 2005. Triple oxygen isotope composition of dissolved O2in the equatorial Pacific: A tracer of mixing, production, and respiration. *Journal of Geophysical Research*, 110.

Hickman, A.E., Moore, C.M., Sharples, J., Lucas, M.I., Tilstone, G.H., Krivtsov, V., Holligan, P.M., 2012. Primary production and nitrate uptake within the seasonal thermocline of a stratified shelf sea. *Marine Ecology Progress Series*, 463, 39-57.

Ho, D.T., Law, C.S., Smith, M.J., Schlosser, P., Harvey, M., Hill, P., 2006. Measurements of air-sea gas exchange at high wind speeds in the Southern Ocean: Implications for global parameterizations. *Geophysical Research Letters*, 33.

Hoefs, J., 2004. *Stable isotope geochemistry*: Springer.

Holley, S.E., Hydes, D.J., 1995. Procedure for the determination of dissolved oxygen in seawater. *James Rennell Centre for Ocean Circulation, Internal Document*, 20, 38.

Holligan, P., leB Williams, P., Purdie, D., Harris, R., 1984. Photosynthesis, respiration and nitrogen supply of plankton populations in stratified, frontal and tidally mixed shelf waters. *Marine ecology. Progress series*, 17, 201-213.

Holt, J.T., James, I.D., Jones, J.E., 2001. An s coordinate density evolving model of the northwest European continental shelf: 2. Seasonal currents and tides. *Journal of Geophysical Research: Oceans*, 106, 14035-14053.

Joint, I., Wollast, R., Chou, L., Batten, S., Elskens, M., Edwards, E., Hirst, A., Burkill, P., Groom, S., Gibb, S., Miller, A., Hydes, D., Dehairs, F., Antia, A., Barlow, R., Rees, A., Pomroy, A., Brockmann, U., Cummings, D., Lampitt, R., Loijens, M., Mantoura, F., Miller, P., Raabe, T., Alvarez-Salgado, X., Stelfox, C., Woolfenden, J., 2001. Pelagic production at the Celtic Sea shelf break. *Deep Sea Research Part II: Topical Studies in Oceanography*, 48, 3049-3081.

Joint, I.R., Pomroy, A.J., 1983. Production of picoplankton and small nanoplankton in the Celtic Sea. *Marine Biology*, 77, 19-27.

Joint, I.R.O., N. J. P Pomroy, A. J 1986. Seasonal production of photosynthetic picoplankton and nanoplankton in the Celtic Sea. *Marine Ecology Progress Series*, 28, 251-258.

Juranek, L.W., Hamme, R.C., Kaiser, J., Wanninkhof, R., Quay, P.D., 2010. Evidence of O2 consumption in underway seawater lines: Implications for air-sea O2 and CO2 fluxes. *Geophysical Research Letters*, 37.

Juranek, L.W., Quay, P.D., 2013. Using triple isotopes of dissolved oxygen to evaluate global marine productivity. *Ann Rev Mar Sci*, 5, 503-524.

Juranek, L.W., Quay, P.D., Feely, R.A., Lockwood, D., Karl, D.M., Church, M.J., 2012. Biological production in the NE Pacific and its influence on air-sea CO2flux: Evidence from dissolved oxygen isotopes and O2/Ar. *Journal of Geophysical Research*, 117.

Jurikova, H., Guha, T., Abe, O., Shiah, F.-K., Wang, C.-H., Liang, M.-C., 2016. Variations in triple isotope composition of dissolved oxygen and primary production in a subtropical reservoir. *Biogeosciences*, 13, 6683-6698.

Kaiser, J., 2011a. Corrigendum to "Technical note: Consistent calculation of aquatic gross production from oxygen triple isotope measurements" published in Biogeosciences, 8, 1793–1811, 2011. *Biogeosciences*, 8, 2561-2565.

Kaiser, J., 2011b. Technical note: Consistent calculation of aquatic gross production from oxygen triple isotope measurements. *Biogeosciences*, 8, 1793-1811.

Kaiser, J., Abe, O., 2012. Reply to Nicholson's comment on "Consistent calculation of aquatic gross production from oxygen triple isotope measurements" by Kaiser (2011). *Biogeosciences*, 9, 2921-2933.

Kaiser, J., Reuer, M.K., Barnett, B., Bender, M.L., 2005. Marine productivity estimates from continuous O2/Ar ratio measurements by membrane inlet mass spectrometry. *Geophysical Research Letters*, 32.

Kara, A.B., Rochford, P.A., Hurlburt, H.E., 2000. An optimal definition for ocean mixed layer depth. *Journal of Geophysical Research: Oceans*, 105, 16803-16821.

Keeling, R.F., Stephens, B.B., Najjar, R.G., Doney, S.C., Archer, D., Heimann, M., 1998. Seasonal variations in the atmospheric O2/N2ratio in relation to the kinetics of air-sea gas exchange. *Global Biogeochemical Cycles*, 12, 141-163.

Knox, M., Quay, P.D., Wilbur, D., 1992. Kinetic isotopic fractionation during air-water gas transfer of O2, N2, CH4, and H2. *Journal of Geophysical Research*, 97, 20335.

Laws, E.A., 1991. Photosynthetic quotients, new production and net community production in the open ocean. *Deep Sea Research Part A. Oceanographic Research Papers*, 38, 143-167.

Laws, E.A., Falkowski, P.G., Smith, W.O., Ducklow, H., McCarthy, J.J., 2000. Temperature effects on export production in the open ocean. *Global Biogeochemical Cycles*, 14, 1231-1246.

Lutz, M.J., Caldeira, K., Dunbar, R.B., Behrenfeld, M.J., 2007. Seasonal rhythms of net primary production and particulate organic carbon flux to depth describe the efficiency of biological pump in the global ocean. *Journal of Geophysical Research*, 112.

Luz, B., Barkan, E., 2000. Assessment of oceanic productivity with the triple-isotope composition of dissolved oxygen. *Science*, 288, 2028-2031.

Luz, B., Barkan, E., 2009. Net and gross oxygen production from O2/Ar, 17O/16O and 18O/16O ratios. *Aquatic Microbial Ecology*, 56, 133-145.

Luz, B., Barkan, E., Bender, M.L., Thiemens, M.H., Boering, K.A., 1999. Triple-isotope composition of atmospheric oxygen as a tracer of biosphere productivity. *Nature*, 400, 547-550.

Luz, B., Barkan, E., Sagi, Y., Yacobi, Y.Z., 2002. Evaluation of community respiratory mechanisms with oxygen isotopes: A case study in Lake Kinneret. *Limnology and Oceanography*, 47, 33-42.

Marra, J., 2002. Approaches to the measurement of plankton production. *Phytoplankton productivity: Carbon assimilation in marine and freshwater ecosystems*, 78-108.

Moat, B.I., Yelland, M.J., Pascal, R.W., Molland, A.F., 2005. An overview of the airflow distortion at anemometer sites on ships. *International Journal of Climatology*, 25, 997-1006.

Moore, C.M., Suggett, D.J., Hickman, A.E., Kim, Y.-N., Tweddle, J.F., Sharples, J., Geider, R.J., Holligan, P.M., 2006. Phytoplankton photoacclimation and

photoadaptation in response to environmental gradients in a shelf sea. *Limnology and Oceanography*, 51, 936-949.

Muller-Karger, F.E., 2005. The importance of continental margins in the global carbon cycle. *Geophysical Research Letters*, 32.

Munro, D.R., Quay, P.D., Juranek, L.W., Goericke, R., 2013. Biological production rates off the Southern California coast estimated from triple O2isotopes and O2: Ar gas ratios. *Limnology and Oceanography*, 58, 1312-1328.

Nicholson, D.P., Stanley, R.H.R., Barkan, E., Karl, D.M., Luz, B., Quay, P.D., Doney, S.C., 2012. Evaluating triple oxygen isotope estimates of gross primary production at the Hawaii Ocean Time-series and Bermuda Atlantic Time-series Study sites. *Journal of Geophysical Research*, 117.

Nightingale, P.D., Malin, G., Law, C.S., Watson, A.J., Liss, P.S., Liddicoat, M.I., Boutin, J., Upstill-Goddard, R.C., 2000. In situ evaluation of air-sea gas exchange parameterizations using novel conservative and volatile tracers. *Global Biogeochemical Cycles*, 14, 373-387.

Nolan, G., O'Boyle, S., 2011. The Influence of Water Column Stratification on Dissolved Oxygen Levels in Coastal and Shelf Waters around Ireland. *Biology & Environment: Proceedings of the Royal Irish Academy*, 110, 195-209.

Osborn, T.R., 1980. Estimates of the local rate of vertical diffusion from dissipation measurements. *Journal of Physical Oceanography*, 10, 83-89.

Palevsky, H.I., Quay, P.D., Lockwood, D.E., Nicholson, D.P., 2016. The annual cycle of gross primary production, net community production, and export efficiency across the North Pacific Ocean. *Global Biogeochemical Cycles*, 30, 361-380.

Palmer, M.R., Inall, M.E., Sharples, J., 2013. The physical oceanography of Jones Bank: A mixing hotspot in the Celtic Sea. *Progress in Oceanography*, 117, 9-24.

Pauly, D., Christensen, V., Guenette, S., Pitcher, T.J., Sumaila, U.R., Walters, C.J., Watson, R., Zeller, D., 2002. Towards sustainability in world fisheries. *Nature*, 418, 689-695.

Poulton, A.J., Stinchcombe, M.C., Achterberg, E.P., Bakker, D.C.E., Dumousseaud, C., Lawson, H.E., Lee, G.A., Richier, S., Suggett, D.J., Young, J.R., 2014. Coccolithophores on the north-west European shelf: calcification rates and environmental controls. *Biogeosciences*, 11, 3919-3940.

Prokopenko, M.G., Pauluis, O.M., Granger, J., Yeung, L.Y., 2011. Exact evaluation of gross photosynthetic production from the oxygen triple-isotope composition of O2: Implications for the net-to-gross primary production ratios. *Geophysical Research Letters*, 38.

Quay, P., Stutsman, J., Steinhoff, T., 2012. Primary production and carbon export rates across the subpolar N. Atlantic Ocean basin based on triple oxygen isotope and dissolved O2and Ar gas measurements. *Global Biogeochemical Cycles*, 26.

Quay, P.D., Peacock, C., Björkman, K., Karl, D.M., 2010. Measuring primary production rates in the ocean: Enigmatic results between incubation and non-incubation methods at Station ALOHA. *Global Biogeochemical Cycles*, 24.

Rees, A.P., Joint, I., Donald, K.M., 1999. Early spring bloom phytoplankton-nutrient dynamics at the Celtic Sea Shelf Edge. *Deep Sea Research Part I: Oceanographic Research Papers*, 46, 483-510.

Reuer, M.K., Barnett, B.A., Bender, M.L., Falkowski, P.G., Hendricks, M.B., 2007. New estimates of Southern Ocean biological production rates from O2/Ar ratios and the triple isotope composition of O2. *Deep Sea Research Part I: Oceanographic Research Papers*, 54, 951-974.

Richier, S., Achterberg, E.P., Dumousseaud, C., Poulton, A.J., Suggett, D.J., Tyrrell, T., Zubkov, M.V., Moore, C.M., 2014. Phytoplankton responses and associated carbon cycling during shipboard carbonate chemistry manipulation experiments conducted around Northwest European shelf seas. *Biogeosciences*, 11, 4733-4752.

Robinson, C., Tilstone, G.H., Rees, A.P., Smyth, T.J., Fishwick, J.R., Tarran, G.A., Luz, B., Barkan, E., David, E., 2009. Comparison of in vitro and in situ plankton production determinations. *Aquatic Microbial Ecology*, 54, 13-34.

Sharples, J., Ellis, J.R., Nolan, G., Scott, B.E., 2013. Fishing and the oceanography of a stratified shelf sea. *Progress in Oceanography*, 117, 130-139.

Sharples, J., Ross, O.N., Scott, B.E., Greenstreet, S.P.R., Fraser, H., 2006. Inter-annual variability in the timing of stratification and the spring bloom in the North-western North Sea. *Continental Shelf Research*, 26, 733-751.

Simpson, J.H., Sharples, J., 2012. *Introduction to the Physical and Biological Oceanography of Shelf Seas*: Cambridge University Press.

Stock, C.A., John, J.G., Rykaczewski, R.R., Asch, R.G., Cheung, W.W.L., Dunne, J.P., Friedland, K.D., Lam, V.W.Y., Sarmiento, J.L., Watson, R.A., 2017. Reconciling fisheries catch and ocean productivity. *Proceedings of the National Academy of Sciences*, 114, E1441-E1449.

Suggett, D.J., MacIntyre, H.L., Kana, T.M., Geider, R.J., 2009. Comparing electron transport with gas exchange: parameterising exchange rates between alternative photosynthetic currencies for eukaryotic phytoplankton. *Aquatic Microbial Ecology*, 56, 147-162.

Sweeney, C., Gloor, E., Jacobson, A.R., Key, R.M., McKinley, G., Sarmiento, J.L., Wanninkhof, R., 2007. Constraining global air-sea gas exchange for CO2 with recent bomb 14C measurements. *Global Biogeochemical Cycles*, 21.

Thomas, C.M., Perissinotto, R., Kibirige, I., 2005. Phytoplankton biomass and size structure in two South African eutrophic, temporarily open/closed estuaries. *Estuarine, Coastal and Shelf Science*, 65, 223-238.

Tiselius, P., Kuylenstierna, B., 1996. Growth and decline of a diatom spring bloom phytoplankton species composition, formation of marine snow and the role of heterotrophic dinoflagellates. *Journal of Plankton Research*, 18, 133-155.

Tortell, P.D., 2005. Dissolved gas measurements in oceanic waters made by membrane Inlet mass spectrometry. *Limnology and Oceanography: Methods*, 3, 24-37.

Tremblay, J.-E., Klein, B., Legendre, L., Rivkin, R.B., Therriault, J.-C., 1997. Estimation of f-ratios in oceans based on phytoplankton size structure. *Limnology and Oceanography*, 42, 595-601.

Wanninkhof, R., 2014. Relationship between wind speed and gas exchange over the ocean revisited. *Limnology and Oceanography: Methods*, 12, 351-362.

Highlights

- Net community and gross production rates during a spring bloom at high resolution.
- Results apply to the mixed layer and below up to the euphotic zone.
- $N(O_2/Ar)$ was spatially heterogeneous and shows autotrophic conditions.
- Gross production rates based on oxygen triple isotopologues were up to 424 mmol m^{-2} d^{-1}.
- Carbon export efficiency much higher on the shelf sea than off the shelf.